https://doi.org/10.15407/knit2022.05.027
UDC 524.7+52-735

V. KHRAMTSOV[1] , PhD student
https://orcid.org/0000-0003-1744-7071
E-mail: vld.khramtsov@gmail.com
I. B. VAVILOVA[2] , Dr. Sci. in Phys.&Math., Prof.
Head of the Department
https://orcid.org/0000-0002-5343-1408
E-mail: irivav@mao.kiev.ua
D. V. DOBRYCHEVA[2] , Ph.D. in Phys.&Math., Senior Scientist
https://orcid.org/0000-0001-5557-3453
E-mail: daria@mao.kiev.ua
M. YU. VASYLENKO[2] , PhD student, Junior Scientist
https://orcid.org/0000-0002-7714-0779
E-mail: vasmax@mao.kiev.ua
O. V. MELNYK[2] , Ph.D. in Phys.&Math., Senior Scientist
E-mail: melnykol@gmail.com
A. A. ELYIV[2] , Ph.D. in Phys.&Math., Senior Scientist
https://orcid.org/ 0000-0001-6215-1048
E-mail: andrii.elyiv@gmail.com
V. S. AKHMETOV[1], Ph.D. in Phys.&Math., deputy-director
E-mail: akhmetovvs@gmail.com
A. M. DMYTRENKO[1] , PhD student
E-mail: astronom.karazin007@gmail.com

[1] V. N. Karazin Kharkiv National University
4 Svoboda Square, Kharkiv, 61000 Ukraine
[2] Main Astronomical Observatory of the National Academy of Sciences of Ukraine
27 Akademik Zabolotny Str., Kyiv, 03143 Ukraine

MACHINE LEARNING TECHNIQUE FOR MORPHOLOGICAL CLASSIFICATION OF GALAXIES FROM THE SDSS. III. THE CNN IMAGE-BASED INFERENCE OF DETAILED FEATURES

This paper follows a series of our works on the applicability of various machine learning methods to morphological galaxy classification (Vavilova et al., 2021, 2022). We exploited the sample of ~315800 low-redshift SDSS DR9 galaxies with absolute stellar magnitudes of $-24^m < M_r < -19.4^m$ at $0.003 < z < 0.1$ redshifts as a target data set for the CNN classifier. Because it is tightly overlapped with the Galaxy Zoo 2 (GZ2) sample, we use these annotated data as the training data set to classify galaxies into 34 detailed features.

In the presence of a pronounced difference in visual parameters between galaxies from the GZ2 training data set and galaxies without known morphological parameters, we applied novel procedures, which allowed us for the first time to get rid of this difference for smaller and fainter SDSS galaxies with $m_r < 17.7$. We describe in detail the adversarial validation technique as well as how we man-

Цитування: Khramtsov V., Vavilova I. B., Dobrycheva D. V.,Vasylenko M. Yu., Melnyk O. V., Elyiv A. A., Akhmetov V. S., Dmytrenko A. M. Machine learning technique for morphological classification of galaxies from the SDSS. III. The CNN image-based inference of detailed features. *Space Science and Technology.* 2022. **28**, № 5 (138). P. 27—55. https://doi.org/10.15407/knit2022.05.027

aged the optimal train-test split of galaxies from the training data set to verify our CNN model based on the DenseNet-201 realistically. We have also found optimal galaxy image transformations, which help increase the classifier's generalization ability.

We demonstrate for the first time that implication of the CNN model with a train-test split of data sets and size-changing function simulating a decrease in magnitude and size (data augmentation) significantly improves the classification of smaller and fainter SDSS galaxies. It can be considered as another way to improve the human bias for those galaxy images that had a poor vote classification in the GZ project. Such an approach, like autoimmunization, when the CNN classifier, trained on very good galaxy images, is able to re-train bad images from the same homogeneous sample, can be considered co-planar to other methods of combating such a human bias.

The most promising result is related to the CNN prediction probability in the classification of detailed features. The accuracy of the CNN classifier is in the range of 83.3—99.4 % depending on 32 features (exception is for "disturbed" (68.55 %) and "arms winding medium" (77.39 %) features). As a result, for the first time, we assigned the detailed morphological classification for more than 140000 low-redshift galaxies, especially at the fainter end. A visual inspection of the samples of galaxies with certain morphological features allowed us to reveal typical problem points of galaxy image classification by shape and features from the astronomical point of view.

The morphological catalogs of low-redshift SDSS galaxies with the most interesting features are available through the UkrVO website (http://ukr-vo.org/galaxies/) and VizieR.

***Keywords**: galaxies: galaxies, morphological classification, methods: data analysis, Convolutional Neural Network, image processing.*

1. INTRODUCTION

Convolutional neural network (CNN) as a machine learning (ML) technique is becoming more and more applicable for astronomical tasks. Its success has been proven sufficiently for big data observational sky surveys: galaxy classification by various properties, pattern recognition image description, celestial body peculiarities' identification, anomalies, transient object detection, etc. The CNNs are very helpful for finding and discovering previously unknown gravitationally lensed quasars [1—3], identifying gravitational lenses [4—7], galaxy-galaxy strong gravitational lenses [8] including in the Dark Energy Survey (DES) imaging data [9] and weak gravitational lensing analysis to create galaxy images as input [10]. The distance moduli estimates benefit from the CNNs utilization in the big data sets, which provide a wide number of galaxy features for learning (see review by Salvato et al. [11]). Bonnett et al. [12] adopted multiple ML methods for determining photometric redshifts with implications for weak lensing from the DES catalog. Amaro et al. [13] compared ANNz2 [14], Bayesian photometric redshift method, and METAPHOR (Machine-learning Estimation Tool for Accurate PHOtometric Redshifts) for KiDS-ESO-DR3 and GAMA DR2 surveys. Similarly, Pasquet et al. [15] used deep learning (DL) for classifying, detecting, and predicting photometric redshifts of quasars in the SDSS. ML and generative adversarial networks (GAN) were used to assign and predict photometric/spectroscopic redshifts within large-scale galaxy surveys with good accuracy [9, 11, 16—20]. The ML approach serves as a basis for restoring galaxy distribution in the Zone of Avoidance and cosmic web as a whole [21—29] and generating dark matter structures in cosmological models [30—32], for extraction of information from noisy maps [33] and image reconstruction of celestial bodies in the whole [34—38], for the task of deblending overlaps between foreground and background galaxies with GAN as CNN technique [39—40] (see, also, scalable ML algorithms and frameworks in [41]). The review of recent trends of ML applicability in cosmology and gravitational wave astronomy can be found in the work by Burgazli et al. [42].

The CNN models have expanded the "optical" range of applications becoming useful for multi-wavelength sky surveys. Among recent studies are as follows: search for blazar candidates in the Fermi-LAT Clean Sample [43]; boosted decision tree for detecting the faint γ-ray sources with future Cherenkov Telescope Array [44—45]; infrared colour selection of Wolf-Rayet candidates in our Galaxy using the Spitzer GLIMPSE catalog [46]; cosmic string searches in 21-cm temperature CMB maps [47]; neural network-based Faranoff-Riley classifications of radio galaxies from the Very Large Array archive [48] and DL classification of compact and extended radio source from Radio Galaxy Zoo [49]; CNN for morphological assignment to radio-detected galaxies with active nuclei [50]. Scaife et al. [51] presented the first application of group-equivariant CNNs to radio galaxy classification and explored their poten-

tial for reducing intra-class variability by preserving equivariance for the Euclidean group on image translations, rotations, and reflections.

The merging galaxies are among the objects to be misclassified. Finding comprehensive samples of such galaxies in different merger stages is significant for studying these long-term processes. In this context, the adversarial training with Domain Adversarial Neural Networks (DANNs) altogether with the Maximum Mean Discrepancy (MMD) method was proposed by Ciprijanovic et al. [52]. Such adaptation techniques allowed these authors to demonstrate a great promise to classify galaxy mergers across domains. As well, to identify peculiar galaxies, an ML system needs to identify forms of galaxies that are not present in the dataset. For such identification of outlier galaxies, the unsupervised ML is proposed by Shamir et al. [53].

Our work follows the previous study [54] (Paper I below), where the photometry-based approach for a binary morphological classification was applied to the SDSS DR9 set of low-redshift ~315800 galaxies. Using various galaxy classification techniques (human labeling, multi-photometry diagrams, and five supervised ML methods), we found that the Support Vector Machine and Random Forest give the highest accuracy (more than 96 % for early and late types). Determining the ability of each method to predict the galaxy morphological type, we verified various dependencies of the method's accuracy on redshifts, celestial coordinates, human labeling bias, the overlap of different morphological features, etc.

This paper aims to obtain the CNN image-based morphological feature classification of 315 782 galaxies with absolute stellar magnitudes of $-24^m < M_r < -19.4^m$ at $0.003 < z < 0.1$ redshifts (with velocities correction on the velocity of Local Group, $V_{\rm LG} > 1500$ km/s). For this, we exploited the annotated data of the Galaxy Zoo 2 (GZ2) project with their crowd-sourcing strategy for volunteers to classify images by answering a series of questions. The sample of the GZ2 galaxies, which overlap with the studied galaxies, served as the training data set for the CNN classifier.

As compared to the paper [55] (Paper II below), this work investigates the problem of differences in the data sets in detail and suggests ways to overcome adversarial validation. We describe in detail a neural network to predict some structural morphological features that can help to classify galaxies with ware used by Walmsley et al. [56]. We analyze the obtained samples of galaxies with different morphological features to obtain their quantitative/qualitative properties and to estimate the efficiency of the CNN classifier.

We describe briefly the target, training, and inference galaxy data sets in Section 2. Methodology consisting of the data preparation, adversarial validation, and CNN morphological classification with the intelligent train-test split via adversarial scores is given in Section 3 (see also Paper II). The general results and discussion are in Section 4, and the conclusion is presented in Section 5.

2. GALAXY DATA SETS

2.1. ***Target data set.*** One of the most crucial principles of ML is comprehending the data you are working with. These design principles are most important at the stage when the data are fed into the chosen algorithms (see, for example, [57]). That is why we used a representative data set of the 315 782 SDSS DR9 galaxies at $z < 0.1$ with the absolute stellar magnitudes $-24^m < M_r < -13^m$, which we name as the target data set (see, in detail, Paper II [55]). We studied it practically as "galaxy by galaxy" in previous works for various tasks [58—68], including the ML photometry-based approach for binary galaxy morphological classification [54] and the catalog of their morphological types [69] obtained with the Support Vector Machine and Random Forest methods. Paper II [55] describes a general methodology for the CNN morphological classification, and a morphological catalog of galaxies classified into five classes according to the GZ2 labeling annotation is published through VizieR [70].

2.2. ***Training and inference data sets.*** To provide the image-based approach for morphological classification of galaxies from the target data set, we used the GZ2 annotated data. To train the neural network, we should have a large number of labeled galaxies images. The target data set of the SDSS galaxies is tightly overlapped with the data from GZ2 [71]. For this reason, we divided our target data set into two data sets. Hereafter, we determine the data set of 143 410

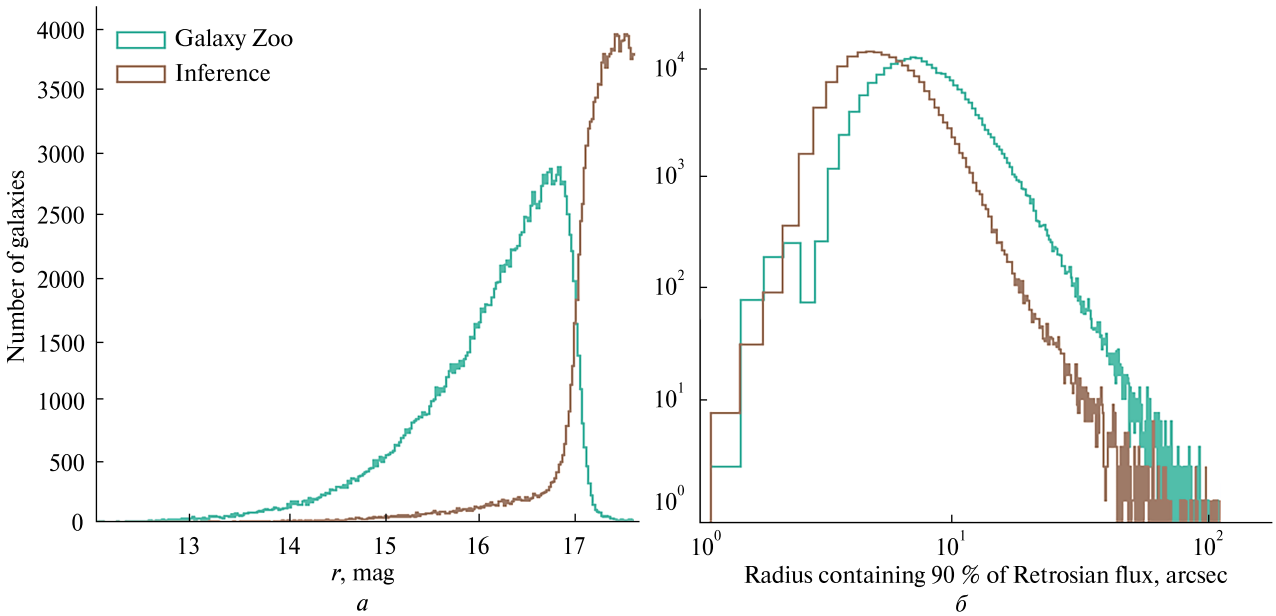

Figure 1. Histograms of the stellar magnitude and Petrosian radius (90 % of the flux) distributions in *r*-band for the training (green) and inference (brown) SDSS galaxy data sets at $z < 0.1$

galaxies, which do not match the GZ2 galaxies, as the "inference" data set. The data set of 172 372 galaxies, which match the GZ2 galaxies, is the "training" data set. The sample from GZ2 contains all the well-resolved galaxies essentially in DR9 with $N = 11923$ galaxies from the Stripe 82 ($11.6 \le m_r \le 17.7$, $0.003 < z < 0.09$), where about of 6800 are at $0.07 < z < 0.09$. We consider galaxies only in normal-depth SDSS imaging and with DR9 spectroscopic redshifts.

We consider two types of morphological classification. The first type is the classification, which includes clearly separable five classes: completely rounded, rounded in-between, cigar-shaped, edge-on, and spiral galaxies. This classification is based on the combinations of precisely labeled GZ2 parameters and, obviously, includes only some part of the training data set. Unlike the first type, the second type of classification works with the 37 galaxy morphological features from the GZ2 and covers all galaxies presented in the training data set.

To form the first type of classification, we used specific criteria which allow us to separate different morphological classes of galaxies [71]. These criteria were listed in Paper II. Besides, we removed seven galaxies that fit in two or more criteria. So, we exploited only those galaxies for training for which the most votes of GZ volunteers were collected. Such constraints are not all-inclusive. The more complete and severe criteria could be used to determine the morphological type of a galaxy as clearly as possible. However, as we discussed in Paper II, the criteria in use are good enough to provide reliable image-based classification.

To form the second type of classification (classification by the morphological features, lower panel in Fig. 3), we used at least one of 37 features of galaxies from the training data set, which are described in the first column of Table 2 and Table 3. Also, we removed three very sparse classes from the consideration ("bulge prominence dominant", "odd feature lens or arc", and "bulge shape boxy") each containing < 10 galaxies. In total, we obtained the training data set of 160 471 galaxies (lower panel, Fig. 3). To test the accuracy of the detailed morphological classification on the faint magnitude end, we also used 16 626 galaxies from the DECaLS (see subsection 3.5).

There is a principal difference between galaxy images in our inference data set and training data set matching the GZ2 catalog. One can see in Fig. 1, that the inference data set is much shallower than

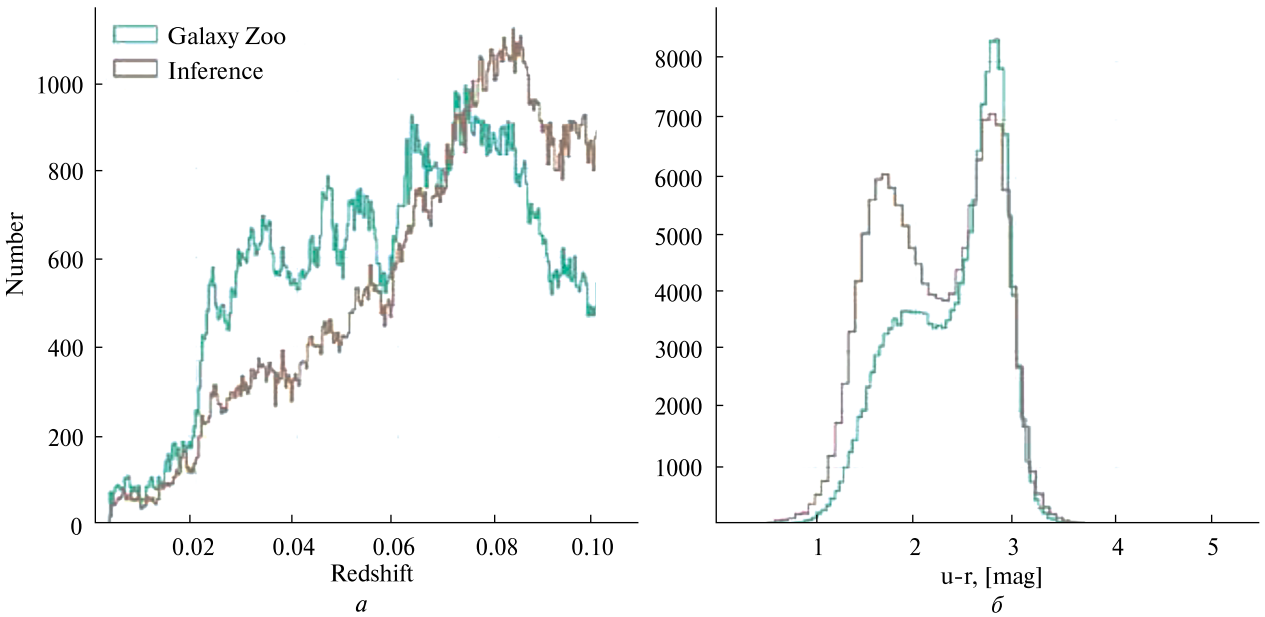

Figure 2. Histograms of the redshifts (*a*) and $u - r$ colour indices (*b*) distributions for the training (green) and inference (brown) SDSS galaxy data sets at $z < 0.1$

the training one. This occurred because the galaxies from the target data set were pre-selected via $m_r < 17.7$ limitation by stellar magnitude in *r*-band. This limitation is related to the 90 % Petrosian flux parameter [72—74]. So, the galaxies, which do not match the GZ2 catalog from the target data set, are, on average, fainter and smaller than galaxies from the training GZ2 data set. In total, 24 547 galaxies from the inference data set have $m_r < 17.7$ (Fig. 1, *a*). The CNN classifier knows nothing that it will work with the inference data set, where galaxies are fainter and smaller than in the training data set. So, it gives us an additional case to study the performance of the image-based classification by providing some additional steps.

Namely, to understand how crucial the shift between training and inference data sets is for the CNN classifier, we use additional test data set. It is based on the image morphological classification of 314 000 galaxies from DECaLS and includes revealed fine morphological features, which are not seen with the SDSS images [74]. With this additional test data set, we identified 16 626 galaxies in our inference data set, which further are used for the approach testing. We note that the morphological classification scheme for the DECaLS is slightly different from that for the GZ2, namely, it is biased towards increasing the detection of bars, measuring bulge size, and distinguishing types of merging galaxies. To align the GZ2 classification used in our study and the DECaLS morphological classification, we removed 15 classes from this data set because the DECaLS morphological classification does not contain some of the GZ2 classes (see Table 2 and Table 3). After this data preparation, we obtained 28 GZ2 feature labels in our additional test data set. Hereafter in the paper, we refer to it as the "deep" test data set.

Other relevant observational parameters are better overlapped among two data sets, see, for example, Fig. 2 with distributions by redshift and (*u-r*) color indices.

2.3. *Images of galaxies.* Images of the training and inference galaxies were requested from the SDSS cutout server. We have retrieved 315 782 RGB images (in PNG format) composed of *gri* bands according to [75] color scaling, each of 100×100×3 pixels. Unfortunately, some of the images were not retrieved for technical reasons (including dead pixels), slightly reducing the training and inference data sets to 172 251 and 136 342, respectively.

We note that scientific image format (like FITS) may be preferable in our task due to the higher amplitude ranges compared to 256 values per band in the simple PNG image. But such a flux sampling is more required for detailed image analyses, for example, gravitational lens modeling, while most of the deep-learning models are working on images with 8-bit amplitudes (see, for example, [76]). Additionally, FITS files from the SDSS may be composed into 5-band images, expanding spectral information, while PNG files are restricted to have three bands only (*gri* in our case). Investigation of this issue is out of scope for our paper, and we used the standard approach of utilizing the SDSS image cutouts for galaxy morphological classification [71].

2.4. ***Implementation.*** All the deep-learning models were implemented using PyTorch[1] and pytorch-image-models[2] libraries. To train the models, we used GPU GeForce GTX 1080Ti.

3. METHODOLOGY, THE CNN IMAGE-BASED GALAXY CLASSIFIER

We exploited CNNs to reveal the morphological classification of galaxies by their images. With this technique, we solve two different classification problems and handle a shift between training and inference data sets.

Usually, CNN consists of layers represented by a sequence of convolutional operations, activation functions, and pooling operations. The principal aim of the CNN is to find such convolutional kernels that are the result of applying the whole CNN to the image finalized in some target value[3]. In our case, the morphological classes and features of galaxies are target values. The CNN architectures use the fully connected layers (instead of convolutional blocks) at the tail. This tail corresponds to the neural network classifier, which transforms the output of the convolutional part into the dense layer, the number of neurons, which is equal to the number of classes.

3.1. ***General approach.*** The scheme of our approach is shown in Fig. 3. First, we divide the studied data set into the training and inference parts (Section 2). Since the inference data set is enormously different from the training one, we have to apply some necessary procedure with a final classification, namely, the adversarial validation[4]. It allowed us not only to probe the difference between the galaxy images in training and inference data sets (middle panel in Fig. 3) but to derive the most suitable method of testing the CNN classifier, which will produce a representative estimation of the quality of the inference data set. This procedure is also significant in our approach for two reasons: the labeled galaxy data sets are biased in stellar magnitude distribution for the training data set (Fig. 1, *a*); such a difference could lead to bias in the final prediction of galaxy classification in the inference data set.

At the second stage of the pipeline, we use CNN to solve the five-class problem described in Section 2. We test our model with the data set defined by the adversarial validation.

Finally, we train a second model to predict the detailed morphological features (e.g., bar, bulge, merging, ring, etc.), which is tested with the adversarial validation and deep test data sets. As a result of a pipeline, we get five morphological classes and 34 detailed morphological parameters for galaxies from the inference data set (third and fourth panels in Fig. 3).

3.2. ***Data preparation and augmentation.*** Stable CNN learning presumes the right scaling or normalization of the input data [81]. We scaled each image I (pixels of which contain values between 0 and 255: $I_{i,j} \in \{0, 255\}$) to the range [–0.5, 0.5] using the scaling equation as follows:

$$\tilde{I}_{i,j} = \frac{I_{i,j} - 127.5}{255}. \qquad (1)$$

Also, we defined many affine transformations for applying to images of galaxies during the CNN learning (so-called image augmentation). In our case, the augmentation helps to introduce the variative nature of galaxies to the CNN methods (because the stan-

[1] https://github.com/pytorch/pytorch

[2] https://github.com/rwightman/pytorch-image-models

[3] A good practical overview can be accessed through http://cs231n.stanford.edu/. We address readers also to works [34, 77—79], where the feature extraction power of CNNs was illustrated in numerical experiments for improving the classification performance, including astronomical image reconstruction.

[4] This method is commonly used in data science competitions, see, e.g., http://fastml.com/adversarial-validation-part-one/ [80].

dard CNNs are not fully invariant to any transformation of the images and have a strong ability to over-fitting). In most cases, this trick improves the generalization ability of CNN producing a less overfitted model on the training data set (see, e.g. [82]). As augmentations, we used random rotation (0°, 90°, 180°, or 270°), random zoom (varying at 100...120 pixels on each axis) with further random cropping of the 100 × 100 region, and random vertical/horizontal flipping of the images of galaxies. This process was applied randomly to each image of a galaxy so that each image of a certain galaxy was put in the CNN as a "new" one reducing the sensitivity of CNN to any galaxy orientation.

These augmentation steps were exploited during the adversarial validation with the CNN classification. We note in advance that after the adversarial validation was produced, we conducted additional data augmentation procedures that helped to learn the CNN classifier better (Section 3.3).

3.3. ***Adversarial validation.*** Having the training and inference data sets (Section 2), we can investigate how the images of galaxies "vary" between these data sets. We trained the CNN on all of these images, passing the class "0" for the inference data set and class "1" for the training one (second panel, Fig. 3).

In this case, the CNN classifier tried to distinguish the training images from images of galaxies from the inference data set, returning the "adversarial score" — the probability of the galaxy being in the training data set. If such a classification accuracy is close to random guessing, one could assume the similarity of the training galaxy images with the inference ones. Moreover, vice versa, when the adversarial classification accuracy largely differs from random guessing (tends to 100 %), one has to investigate the difference between the training data set and the inference one to predict the classes of inference objects correctly. The adversarial score is a measure of how an individual galaxy is similar to the training data set (larger scores correspond to larger similarities with galaxies from the training data set). The effect of dissimilarity is due to the different observed parameters of galaxies from the training and inference data sets. We used the full GZ2 data set as a training data set (comprising 172 372 galaxies) with adversarial class "1".

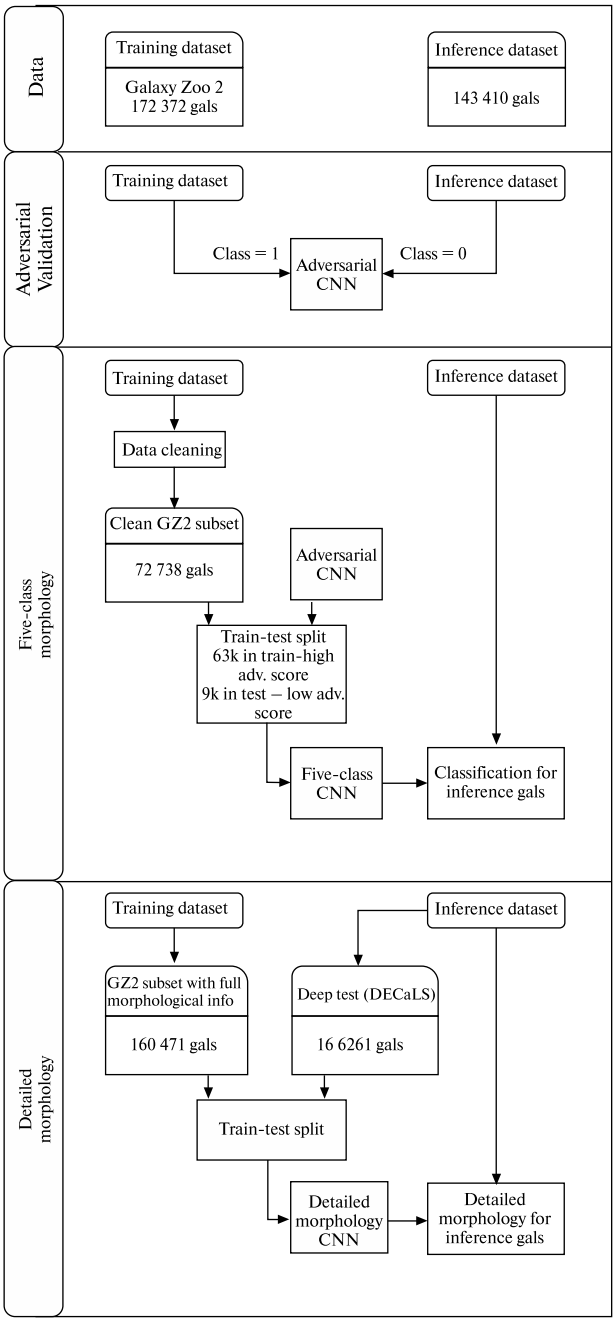

Figure 3. Scheme of the image-based approach for morphological classification of galaxies. The methodology consists of the data preparation of GZ2 training and SDSS DR9 inference data sets, image augmentation, adversarial validation, five-class CNN classification with intelligent train-test split via adversarial scores, CNN detailed morphology by 34 image galaxy features with DECaLS deep test. The algorithm has resulted in the classification of the inference galaxy data set

We employed ResNet-101 [83] as a model, where the convolutional part was completed by the two layers of neurons with 128 and 2 neurons in each layer respectively. After the first layer of neurons, we put on the Leaky Rectified Linear Unit activation function. The last layer that returns the probabilities of being in the training or inference dataset was supplemented by the "softmax" activation function. As an optimizer, we used Adam with an initial learning rate of 5×10^{-3}; the optimizer minimized the categorical "crossentropy loss function". In this way, we tried a single ResNet-101 model as a baseline approach and obtained a good accuracy for GZ2 vs inference classification. We did not vary models because the aim is not to have a performance as higher as possible. The trained model is just a key-performance indicator for each galaxy, and its outputs were used as the proxy metric to understand the similarity between the target (not GZ) data set and each galaxy or its augmented version.

The whole input set consisted of ~170 000 galaxies from the GZ2 training data set and 136 000 galaxies from the inference one. We have trained the model on 75 % of the input data and validated it on the rest part of the galaxies. We applied standard data augmentation procedures to the training images described in Section 3.2. The model was learned during 12 epochs. If the overall classification accuracy of galaxy images from the validation data set did not increase during three epochs, we decreased the learning rate by a factor of 0.1. Finally, we used the model that provided the best overall accuracy (91.28 % on the validation data and 91.67 % on the training one).

For our task, we obtained the accuracy of adversarial classification above 90 %. So, the inference dataset contains galaxies with morphological properties which are not inherited from the training set. One can see in Fig. 4, *a* that the adversarial score is relatively high for a few galaxies only from the inference data set. This agrees with our observation that inference galaxies are fainter (Fig. 1, *a* and smaller (Fig. 1, *b*) than galaxies from the training data set.

We highlight that the resulting adversarial classification accuracy is not a result of over-fitting. Specifically, we randomly split the GZ2 training plus inference data sets into two parts. One of which was used to train the adversarial CNN and another to validate it. The CNN scored the same adversarial accuracy for these subsets (91 %). So, according to the adversarial result, we can conclude that our training data set contains galaxies, properties of which are not common with the inference one. This means that any validation of the morphological classifier has to be done with the galaxies from the training data set, which have a low adversarial score.

There is a typical danger case of over-fitting when an ML model is well performed on the training data set but is not able to generalize to new, previously unseen data. This effect may be controlled through the train-test splitting. In such a way, a portion of the data (called the test data) is set aside to be used only to assess the performance of the trained model and is not included in the training data set. To do so, we randomly choose 9 000 galaxies with an adversarial score higher than 0.7 from the training data set of 72 738 galaxies (comprising five different morphological classes). We picked up the best threshold 0.7 with a simple search taking into account the largest accuracy (see Fig. 4, *a*); other thresholds result in lower separation quality. Within this train-test split, the test part of training galaxies (9 000) was used to validate the morphological CNN classifier, and the rest part of the galaxies (63 738) to train CNN classifier (third panel, Fig. 3). It allows to understand the CNN ability to generalize on data it has never seen before, namely on the galaxies, which are similar to the inference dataset according to their adversarial score.

To train the CNN classifier for the prediction of the classes of fainter and smaller galaxies, we have added the following transformations of images to the defined data augmentation procedures (see subsection 3.2 and Eq. 1):

$$\tilde{I}_{i,j} = \frac{k \times S(I_{i,j}, m) - 127.5}{255}, \qquad (2)$$

where $S(I_{i,j}, m)$ is a function changing the size of the image by m times, and k is an intensity-scaling coefficient. We implemented the size-changing function as simple zooming out of the image (into the new image with axes $(100 \times m) \times (100 \times m)$ pixels, where $0 < m < 1$), followed by mirror reflection of the image to fill up the missing $100 \times (1 - m)$ pixels along the borders. In turn, the intensity of pixels for each image was reduced by a factor of $0 < k < 1$ (Eq. 2).

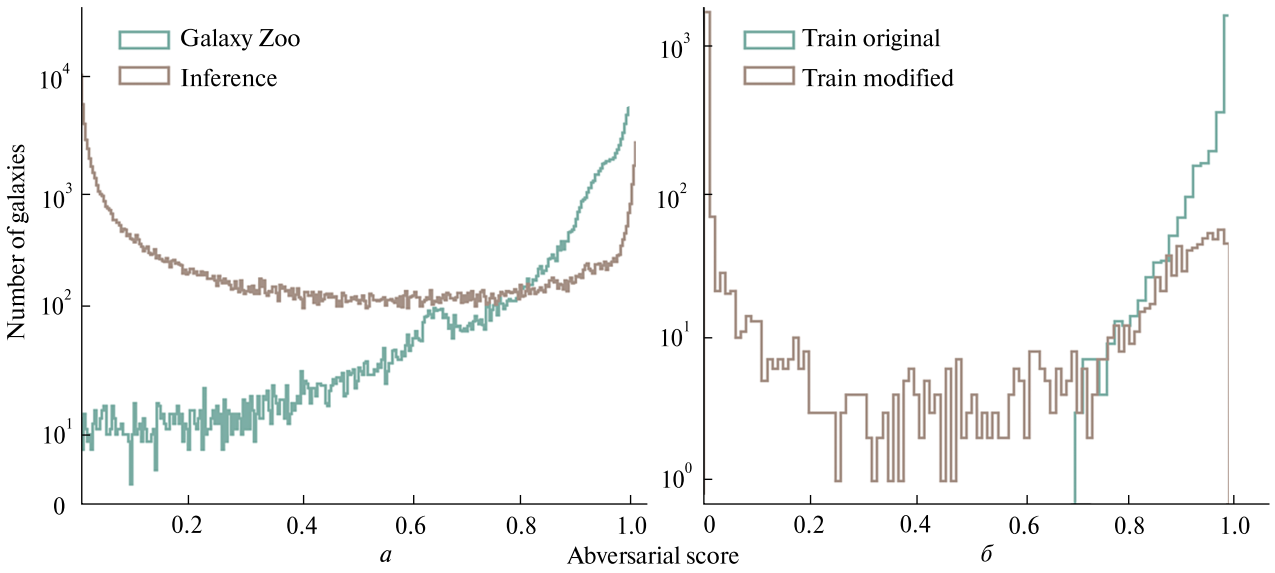

Figure 4. Histograms of adversarial score distributions (*a*). The inference galaxy data set (brown) and for elliptical and spiral galaxies from the GZ2 training data set. Adversarial score is close to 1 if the galaxy is similar to the galaxy from GZ2 training data set (*b*). A random subset of 3000 images from the training data set revealed from original SDSS images (green) and images with modified sizes and intensities of galaxies as $k = 0.8$, $m = 0.7$ from Eq. 2 (brown)

The augmentation procedures we implemented allow us to transform the image of the galaxy, simulating a decrease in magnitude and size as well as veiling it as the galaxy image from the inference dataset. For example, applying these transformations ($k = 0.8$, $m = 0.7$) to the 3 000 random images from the training data set with the adversarial score > 0.7, we observed the shift of the adversarial score distribution towards zero value (see Fig. 4, *b*). The histogram of the adversarial score distribution, especially for lower values, gives direct confirmation in the support of such transformations. This trick with image transformations improves the accuracy of the result emulating the training galaxies to be more similar to the galaxies from the inference data set according to the adversarial scores. In this way, we do not investigate effects caused by different "modalities" (training / inference); instead, we built a technique to prevent prediction biases. In other words, we solved the domain adaptation problem but with manually in-built heuristics (changing angular sizes and intensity of images of training galaxies).

3.4. ***CNN five-class morphological classifier.*** The next step of our pipeline was the morphological classification with CNN on training galaxy images (third panel, Fig. 3). The principal difference between our approach and the existing ones (see, for example, recent works [56, 84—86]) is the usage of

1) the pre-defined training-test split through adversarial validation of the classification accuracy on the inference-like test set, and

2) the specific data augmentation, which allowed us to decrease the difference in galaxy images related to the stellar magnitudes between the GZ2 and inference data sets.

The procedure of training the CNN with the overall accuracy of 89.3 % on the test data set of 9 000 galaxies is described in Paper II. As for the data augmentation procedures, we used the standard techniques described in Section 3.2 and the intensity and size reduction of the galaxy images described in the previous subsection. For each galaxy from the training data set, we randomly sampled k and m from the uniform distribution within (0.6, 1.0) and (0.5, 1.0) ranges (Eq. 2), respectively. Data augmentation was applied to the training data set only. The confusion matrix of the distribution of prediction probabilities of all the classes is in Ta-

ble 1 of Paper II. One can see that accuracy is not dominated by scores for morphological classes with higher numbers of galaxies.

Table 1. **Accuracy scores of backbone models for the five-classes of CNN morphological classification on the validation data**

Architecture	References	Accuracy
ResNet-50	[83]	0.821
ResNet-101	[83]	0.832
ResNet-152	[83]	0.826
InceptionV3	[88]	0.937
InceptionResNetV2	[89]	0.962
DenseNet-121	[87]	0.960
DenseNet-169	[87]	0.959
DenseNet-201	[87]	0.966
NASNetLarge	[90]	0.929
VGG16	[91]	0.909
Xception	[92]	0.956

Similar to the model for the adversarial validation, the tail of CNN models was completed by the two dense layers of neurons (with the number of neurons equal to 128 and 5, respectively) followed after the global max-pooling. The activation functions at the tail of the CNN model were the same as in adversarial validation. As an optimizer, we also used the Adam with an initial learning rate of 10^{-4}; the optimizer minimized the categorical "crossentropy loss function".

CNN models were trained during 40 epochs. Moreover, during the learning, we decreased the learning rate value if the loss on the validation dataset was not decreased after four epochs. The eventual classification accuracy of the validation data set for all models is shown in Table 1. As the result of a comparison between these models, we decided to use DenseNet-201 [87], which shows the highest accuracy on the "unseen" validation (96.6 %) and test (89.3 %) data sets.

Table 2. **Quality of inference morphological feature on the test data sets of galaxies (see, description in the text of this paper)**

Parameter	ROC^{test}_{NOAUG}	ROC^{test}_{AUG}	ROC^{test}_{diff}	$ROC^{deep\ test}_{NOAUG}$	$ROC^{deep\ test}_{AUG}$	$ROC^{deep\ test}_{diff}$	Threshold	N, all data	N, inf. data
Smooth	89.25 %	88.59 %	–0.66 %	86.06 %	86.84 %	0.78 %	0.1	107657	51911
Features or disk	92.54 %	91.88 %	–0.66 %	85.63 %	85.43 %	–0.20 %	0.3	138207	58796
Star or artifact	95.36 %	97.63 %	2.28 %	57.70 %	51.43 %	–6.27 %	0.05	220	73
Edgeo yes	98.81 %	98.65 %	–0.16 %	87.35 %	88.26 %	0.91 %	0.05	34420	14489
Edgeon no	97.21 %	96.82 %	–0.39 %	75.53 %	76.41 %	0.88 %	0.25	72843	19088
Bar	93.99 %	92.41 %	–1.57 %	57.54 %	57.54 %	0.00 %	0.05	29892	6276
No bar	90.69 %	89.80 %	–0.90 %	68.82 %	68.61 %	–0.21 %	0.2	86836	27861
Spiral	93.40 %	92.88 %	–0.52 %	78.97 %	79.48 %	0.51 %	0.15	65709	17741
No spiral	86.30 %	84.78 %	–1.52 %	—	—	—	0.05	69303	20603
No bulge	98.36 %	98.35 %	–0.01 %	65.09 %	69.03 %	3.94 %	0.05	6970	4046
Bulge just noticeable	90.89 %	89.75 %	–1.14 %	—	—	—	0.05	39627	14926
Bulge obvious	90.55 %	89.07 %	–1.49 %	62.45 %	64.31 %	1.86 %	0.05	27115	10018
Bulge dominant	—	—	—	—	—	—	—	—	—
Odd yes	94.78 %	93.37 %	–1.41 %	—	—	—	0.05	41334	17601
Odd no	84.62 %	83.51 %	–1.11 %	—	—	—	0.45	170898	79134
Completely round	96.17 %	95.60 %	–0.58 %	93.09 %	93.51 %	0.43 %	0.15	75844	35669
Rounded in between	92.31 %	91.46 %	–0.85 %	82.73 %	82.84 %	0.11 %	0.2	125734	70389
Cigar shaped	97.96 %	97.73 %	–0.23 %	97.24 %	97.46 %	0.22 %	0.1	60395	30351
Ring	96.97 %	96.43 %	–0.54 %	—	—	—	0.05	13882	1346
Lens or arc	—	—	—	—	—	—	—	—	—

3.5. ***Detailed galaxy morphology classification.*** We used another CNN model to predict 34 detailed morphological parameters of galaxies from the inference data set. This model exploited DenseNet-201 [87] as the backbone model with the included fully connected layers at the top (namely, global max-pooling, fully-connected layer with 512 neurons, and classification fully-connected layers with 34 outputs). We put Rectified Linear Unit activation after the first fully-connected layer and sigmoid activation after the last classification of fully-connected layers. The model was trained with the Adam optimizer, which minimized the "binary crossentropy loss" function. We solved a multi-label classification problem: one object may have a few features. So, we did not use the "softmax" activation function after the classification layer; instead, we treated each class separately and solved binary-classification for each label. This configuration looks suitable for solving the multi-label problem when we do not need to predict probability distribution over all classes to infer the single class for a single sample (fourth panel, Fig. 3).

We provide below in Table 2 and Table 3 two resulting accuracy scores measured with the ROC AUC classification quality metric [93] to predict 34 morphological features of galaxies. The names of features are in the first column. The next columns correspond to the quality metrics (ROC AUC), ROCtest for GZ2 test data set, and ROCdeep test for the DECaLS. We provided three scores for each data set: with and without adversarial augmentation and the difference between both scores. The last three columns: threshold; a number of galaxies matching this criterion from all the target data set and the inference data set, respectively. Empty cells correspond to the missed features. The sum numbers in columns 9 or

Table 3. (continue). **Quality of inference morphological feature on the test data sets of galaxies (see, description in the text of this paper)**

Parameter	ROC^{test}_{NOAUG}	ROC^{test}_{AUG}	ROC^{test}_{diff}	$ROC^{deep\ test}_{NOAUG}$	$ROC^{deep\ test}_{AUG}$	$ROC^{deep\ test}_{diff}$	Threshold	*N*, all data	*N*, inf. data
Disturbed	72.27 %	68.55 %	–3.72 %	—	—	—	0.15	0	0
Irregular	96.74 %	96.94 %	0.20 %	—	—	—	0.05	9432	6369
Other	95.93 %	89.20 %	–6.74 %	—	—	—	0.05	1442	624
Merger	91.79 %	88.89 %	–2.90 %	—	—	—	0.05	2575	738
Dust lane	99.39 %	99.40 %	0.02 %	—	—	—	0.05	588	67
Bulge shape rounded	96.73 %	96.27%	–0.47 %	67.18 %	67.26 %	0.08 %	0.05	32280	12835
Bulge shape boxy	—	—	—	—	—	—	—	—	—
Bulge shape no bulge	98.65 %	98.52 %	–0.13 %	71.61 %	71.46 %	–0.16 %	0.05	19570	10867
Arms winding tight	89.45 %	88.60 %	–0.85 %	72.25 %	72.29 %	0.04 %	0.05	22180	5414
Arms winding medium	75.33 %	77.59 %	2.26 %	69.91 %	71.57 %	1.66 %	0.05	304	86
Arms winding loose	94.95 %	94.41 %	–0.54 %	69.03 %	69.95 %	0.92 %	0.05	8411	3269
Arms number 1	85.56 %	83.30 %	–2.26 %	60.22 %	61.83 %	1.61 %	0.05	445	188
Arms number 2	90.55 %	89.99 %	–0.56 %	76.33 %	76.62 %	0.30 %	0.05	69229	22061
Arms number 3	93.54 %	93.47 %	–0.07 %	70.14 %	68.55 %	–1.58 %	0.05	889	78
Arms number 4	93.84 %	85.45 %	–8.39 %	54.95 %	56.96 %	2.01 %	0.05	82	3
Arms number more than 4	97.79 %	97.51 %	–0.27 %	—	—	—	0.05	55	4
Arms number cannot tell	86.13 %	86.07 %	–0.06 %	—	—	—	0.05	7683	1329

10 may not be equal to the total number of galaxies: one galaxy can have features in several classes, and it is also possible that there are galaxies that do not fit any criterion.

These tables allow comparing this score for the model trained with adversarial augmentations (Section 3.2) and for the model trained without these augmentations. Such a comparison should be useful to understand the degree of influence of image augmentations on the classification quality of the trained model. Scores are given for two test data sets: 1) for the data set of 9000 galaxies and 2) for the DECaLS galaxy data set. As one can see in these Tables, for the case of the GZ2 test data set, the scores, in general, are lower on tests for the model, trained with "flux weakening" and "size reduction" augmentations. This effect is explained by the similarity of the train and test data sets because due to the object selection in the GZ2 project, we are not able to sample a satisfactory amount of faint and small galaxies to test on. And thus, our adversarial augmentations shifts the training data set distribution with respect to the test data set.

At the same time, we note the improvement in the classification of the DECaLS galaxies. The scores overall are much lower than in the case of our GZ2 test data set. It may be explained by the revealing finer structure of morphology with DECaLS: galaxies, which have some class in the GZ2, may be classified in another class with the DECaLS. But applying a model trained with adversarial augmentations leads to increasing the classification quality (except star or artifact class).

4. GENERAL RESULTS AND DISCUSSION

There are many classifiers for sorting galaxies by morphological type and features, but each has its own drawbacks. For example, spectroscopy classification requires different methods to define simultaneously similar spectra for quiescent/starburst and star-forming galaxies [94, 95] or emission-line galaxies [96]. As well, a photometry-based approach gives an error when trying to classify red spirals and blue ellipticals [64, 67, 97—100], i.e., galaxies with a high content of old stars or interacting galaxies which affect the photometric characteristics of each other [101—104]. Analyzing our obtained results and data products let us discuss several issues related to the CNN image-based galaxy classification.

4.1. ***Accuracy.*** We applied CNN classifier to the studied low-redshifts SDSS galaxies and seized two sets of parameters: predictions of beings in one of five classes and to have one of 34 detailed morphological features using the GZ2 labeling. We remind that the five GZ morphological classes are relevant to certain galaxy morphological types, e.g., T-types by de Vaucouleurs. Also, the human bias, which is caused by the GZ volunteers' answers in the decision tree, affects the classification accuracy. It is discussed by many authors in different aspects (see, if interesting, "Astronomy Blog. Galaxy Zoo and human bias" [5]. We refer to the paper by Cabrera et al. [105], where the metric for human labeling measuring in the case of low-redshift spiral/elliptical galaxies is proposed in the frame of label's comparison between experts, GZ volunteers, and ML models. Hart et al. [106] developed a reliable method for defining spiral galaxies, which eliminates the redshift-dependent bias in the GZ2 volunteer's answers. It was taken into account "by modeling the vote fraction distributions as a function of redshift, and correcting the higher redshift vote distributions to be as similar as possible to equivalent vote distributions at low redshift."

We exploited the GZ2 annotated data as by Willett et al. [71], which can possess a worse bias for, as an example, the late-type galaxies (spiral) as compared with the data by Hart et al. [106]. Of course, the exploiting more and more unbiased data for training should improve the accuracy of the CNN classifier, see, for example, Tarsitano et al. [107], where this debiasing technique is applied for "disk and smooth" galaxies. Nevertheless, in general, our method is on par with the most contemporary level of morphological classification performance, attaining the accuracy of 83.3...99.4 % in depending on the morphological galaxy feature (Table 2 and Table 3). Such an overall value of the accuracy is in a good agreement with the one obtained in work by Walmsley et al. [56], who used Bayesian CNN to study Galaxy Zoo volunteer responses and achieved coverage errors of 11.8 % within a vote fraction deviation of 0.2.

[5] https://www.strudel.org.uk/blog/astro/000758.shtml

If consider the attained accuracy for certain morphological types of galaxies, we note the work by Gauthier et al. [108], who applied both supervised and unsupervised methods to study the Galaxy Zoo data set of 61 578 pre-classified spiral, elliptical, round, and disk galaxies. They attained 94 % accuracy for galaxies to be associated with each of these four classes and noted the correlation of variation of galaxy images with brightness and eccentricity. Among other relevant works, we note one by Barchi et al. [109], who used DL and traditional ML techniques for binary distinguishing of elliptical/spiral galaxies and created a morphological catalog of 670 560 galaxies at $z < 0.1$, where the input data were taken from the SDSS DR7 (Petrosian magnitude in *r*-band < 17.78). They developed a non-parametric galaxy morphology system (CyMorph). The Decision Tree, Support Vector Machine, and Multilayer Perceptron produced 98 % of overall accuracy. The CNN method (GoogLeNet Inception) with the imbalanced data sets and twenty-two-layer network resulted in 98.7 % overall accuracy for this binary morphological classification. Mitta et al. [110] introduced the data augmentation-based MOrphological Classifier Galaxy using CNN (daMCOGCNN) and obtained a testing accuracy of 98 % on the data sets of 4 614 images from the SDSS, Galaxy Zoo challenge, and Hubble Image Gallery.

4.2. ***Train-test split. Transformation of images by intensity and size. Adversarial validation.*** We revealed that adversarial validation is very helpful when the labeled data sets are biased in magnitude distribution for the training data set, and such a difference could bias the final prediction of the classifier on the inference data. So, we apply the adversarial validation method to analyze the homogeneity of the two data sets (inference and training). As a result, the galaxies were selected from the training data set that most closely coincided with the inference data set, and the images were normalized to be similar.

The principal difference of our approach is the pre-defined training-test split through adversarial validation of the classification accuracy on the inference-like test data set (Fig. 3). The deal with testing classification quality on different distributions (e.g., between training and target datasets) has a few implementations for galaxy morphology classifications ([86, 111—113]). Below we note several of them.

Gauci et al. ([114]) used decision tree algorithms trained on *gri* photometric information (color indices, shape parameters) to distinguish between spiral and elliptical galaxies or star/ unknown galactic objects from SDSS DR7 following the GZ annotated data. They revealed that the incorrectly classified spiral and elliptical samples are very faint in magnitude. Our approach with adversarial augmentation and revealing differences between training and inference datasets allows us to avoid this problem.

The transfer learning approach to fine-tune the CNN on a dataset, different from the training one, has been recently acted by Ghosh et al. [112] in their CNN classifier for bulge- and disk-dominated galaxies of the SDSS and Cosmic Assembly Near-Infrared Deep Extragalactic Legacy Survey (CANDELS). The inclusion of this procedure allowed them to overcome the problem of non-accurate predictions on the unseen datasets by fine-tuning the network on the target dataset. Dominguez-Sanchez et al. [115] created a morphological catalog for ~670 000 SDSS-galaxies in two options (T-type, related to the Hubble sequence, and GZ2 types). They obtained the highest accuracy (>97 %) when applying the same parameters to a test data set as those used for the training data set.

But the labeled data from the target distribution is an essential condition to conduct the transfer learning. We handled this limitation simply by imposing the required transformations into the training dataset, preventing the need to label the target galaxies.

Lin et al. [116] used the Vision Transformer model, which operates better at classifying smaller-sized and fainter galaxies (in comparison to the CNN). This improvement is caused, probably, by the architecture change from the CNN to the attention-based model — because transformers usually work better with a training dataset increasing, and, at the same time, these challenging types of galaxies were dominated in their training dataset. The results related to the fainter have a special interest when compiling the samples of low surface brightness galaxies [117—120]. Lin et al. applied thresholds on a series of voting GZ2 questions [71] but considered eight classes: round elliptical, in-between elliptical, cigar-shaped elliptical, edge-on, barred spiral, unbarred spiral, irregular, and merger on the data set of 155 951 images of galax-

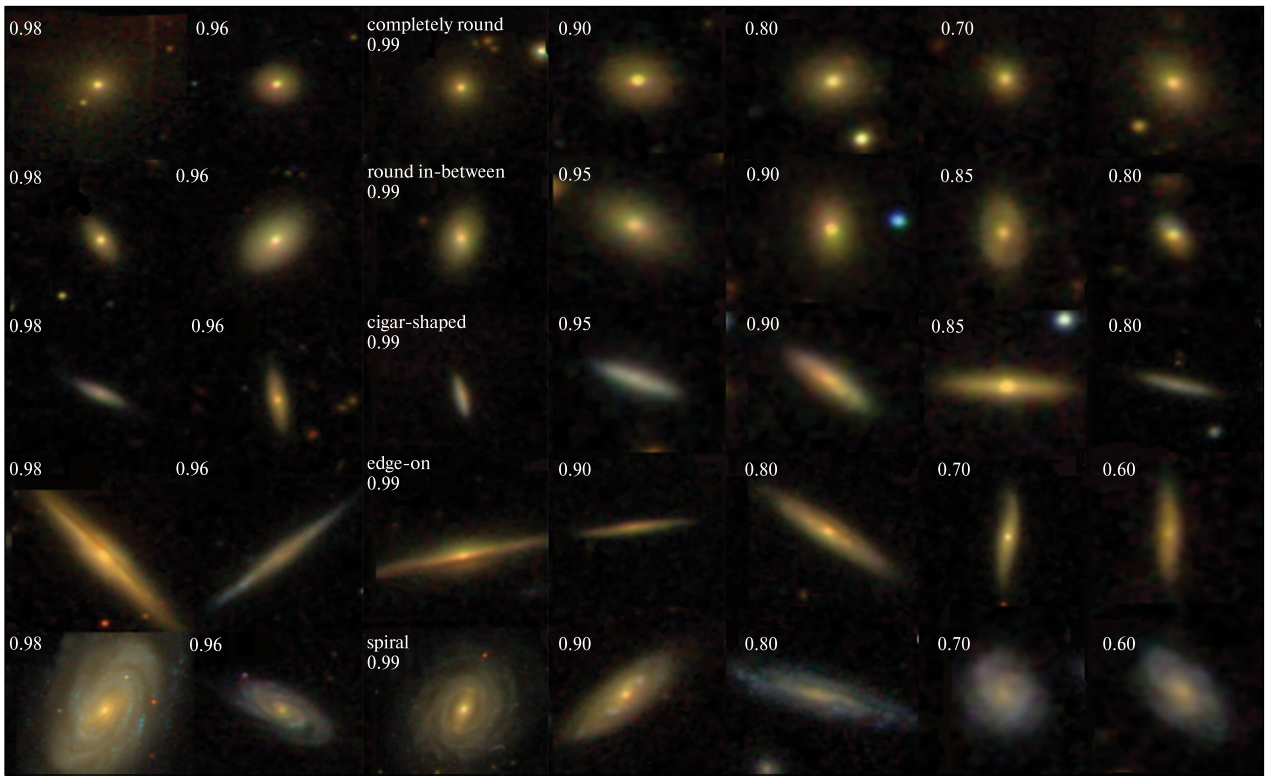

Figure 5. A set of the inference galaxies (3—7 columns) with their two nearest neighbours from the GZ2 training data set (1—2 columns). Each row represents the morphological class, which is intrinsic to the galaxy from the training data set. A value of the probability of being this galaxy in a given class is pointed in the left upper corner of each image

ies [116]. These authors attained the accuracy (with equal class weights) from 68.7 % to 90.7 % in dependence on the class, excepting irregular (41.3 %) and mergers (53.1 %). Dieleman et al. used similar to our data augmentation when provided the GZ decision tree model to predict probabilities for each of 34 answers of the GZ volunteers for the evaluation set of 79 975 SDSS galaxy images [82]. They selected the subset of images for which at least 50 % of volunteers answered the question. Exploiting translational and rotational invariation of galaxy images via data augmentation and keeping the center of the galaxy as the most informative part, they also used random rescaling, flipping, and brightness adjustment. For images with high agreement among the GZ participants, their model provides an accuracy of more than 99 % for most questions.

The aforementioned results show the success of a standard data augmentation technique, while sophisticated augmentations — to adapt the training set to the inference one — are also effective, as we demonstrate in this paper.

4.3. ***CNN classification by five morphological classes of galaxies.*** Assuming that a galaxy is in a certain class if the probability is the highest one, we have found (Paper II) that the inference data set comprises 27 378 completely round (with the probability of 83 %), 59 194 round in-between (93 %), 18 862 cigar-shaped (75 %), 7 831 edge-on (93 %), and 23 119 spiral (96 %) galaxies (see, examples, in Fig. 5, similarity search). The Catalog of 315 776 SDSS DR9 galaxies at $z < 0.1$ with image-based morphological classification by five classes is available through the UkrVO website[6] and VizieR [70] to be supplemented with Paper II [55]. It contains the CNN morphologi-

[6] http://ukr-vo.org/starcats/galaxies/gal_SDSSDR9_z_to_0.1_morph_5_classes.csv

cal classification of 72738 galaxies from the training GZ2 data set, 143410 galaxies from the inference data set (the faintest galaxies of the studied sample), 99528 galaxies from the GZ2 sample that did not pass the selection according to the criteria of the most votes of GZ2 volunteers and for which their morphological class was reassigned by the CNN classifier.

In this way, we have shown for the first time that implication of the CNN model with adversarial validation and size-changing function simulating a decrease in magnitude and size (data augmentation) significantly improves the classification of smaller and fainter SDSS galaxies with $m_r < 17.7$ in *r*-band (Fig. 4, *a*). One can see in Fig. 1, *a* that the fainter end of distribution of the target data set by magnitude is occupied by galaxies from the inference data set only. As well, we demonstrated another way to improve the human bias for those galaxy images that had a poor vote classification in the GZ project. Such an approach, like autoimmunization, when the CNN classifier trained on very good images is able to retrain bad images from the same homogeneous sample, can be considered co-planar to other methods on improving human bias, e.g., the method proposed by Hart et al. [106].

It is relevant to compare our results with work by Zhu et al. [121], in which the ResNet model was exploited to classify galaxies into five classes annotated by GZ2 and CNN classifier was compared with Dieleman et al. [82], AlexNet, VGG, and Inception networks. The samples were pre-selected in a specific morphology category with their appropriate thresholds [71] in dependence on the number of volunteers' votes. These authors attained overall classification accuracy of 95.21 % and the accuracy of each class type of 96.68 % for completely round, 94.42 % for round in-between, 58.62 % for cigar-shaped, 94.36 % for edge-on, and 97.70 % for spiral. We had a comparable classification performance with a worse output for completely round and a better output for cigar-shaped classes. Gupta et al. [86] provided a classification of GZ2 galaxy images on five morphological classes as in our work. They trained Neural ordinary differential equations with Adaptive Checkpoint Adjoint and compared them against the ResNet CNN model: an accuracy of 91...95 % depending on the image class is in agreement with our results.

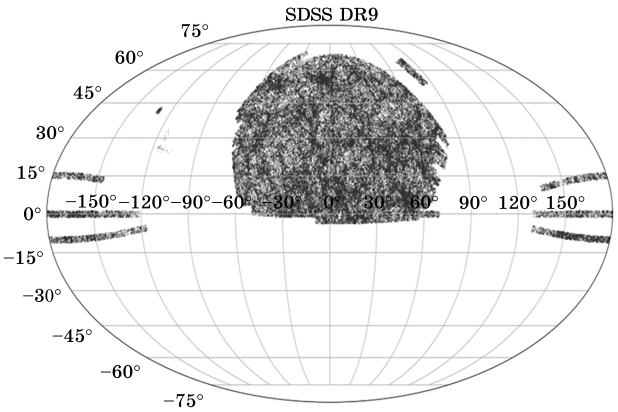

Figure 6. Distribution of galaxies classified by CNN as belonging to the round in-between morphological class in the sky

Yet one point of the discussion is related to the distribution of galaxies in the sky and by redshift. For example, Dhar and Shamir [122] demonstrated that the training of a deep CNN is sensitive to the context of the training data, such as the location of the objects in the sky. They found statistically significant bias in the form of cosmological-scale anisotropy in the distribution of elliptical and spiral galaxies, which affect the deep CNN model. They experimented with Pan-STARRS and SDSS data and noted that such unbalancing is linked to the training and test samples of galaxies, which were imaged in different parts of the sky. We analyzed the distribution of galaxies in our catalogs and have not found that galaxies of a certain morphological class (or morphological feature) have a preferential distribution in their location in the sky (see as an example, Fig. 6 for the most numerous round-in between class and Fig. 2, *a* for the training and inference data sets. There are no differences between classes in distribution by redshift (Fig. 7).

To compare photometry-based and image-based approaches to the same data set of low-redshift galaxies, we collected the classification output of four methods in Table 4. There are results of classifications by the CNN model into five morphological classes [55]; photometry multi-parametric diagram (MPD) into elliptical, spiral, and irregular galaxies [58, 60]; machine learning with Random Forest (RF) and Support Vector Machine (SVM) into early and late morphological types [54]. We inserted the num-

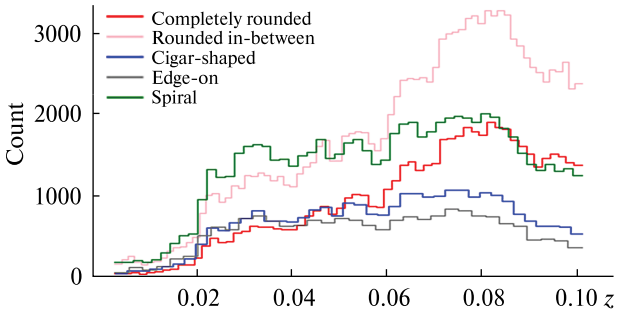

Figure 7. Distribution of galaxies classified by CNN into five morphological classes by redshift

ber of only those galaxies that have the maximum probability of belonging to one or another morphological class [70]. One can see that three photometry-based methods have comparable overall accuracy with an intrinsic error of less than 0.3 % between RF and SVM [54] as well as less than 4 % between MPD (here, late type is Sp+Irr) and machine learning methods. The latter error is explained mostly by the effect of blue elliptical and red spiral galaxies [58]. There is a general agreement between the early type of galaxies classified by photometry methods and "round-in-between + completely round" types of galaxies as well as between late-type galaxies and "spiral + round in-between".

We matched the galaxies of late morphological types classified by Support Vector Machine (SVM) and Random Forest (RF) [69] and the galaxies classified in this work by CNN as edge-on and spiral as the most relevant morphological types. Namely, we selected ~50 000 galaxies with a CNN probability of being spiral from 0.77 to 0.99 (Table 2 and Table 3). Their labeling obtained by SVM and RF methods says that 10.5 %, and 8.8 % among them, respectively, are of early morphological type (elliptical). We inspected these misclassified galaxies and found that they are mostly large nearest spiral galaxies with a massive red center region.

We also selected ~12 000 edge-on galaxies with the same CNN probability: also having a redder color and larger redshifts. The comparison in Table 4 shows significant segregation of galaxies classified by five GZ2 morphological classes between the adopted morphological types. This complicates the work of the CNN classifier to reveal the real morphology of galaxies. The statistical comparison of these results with the results of the CNN detailed morphology of the same five classes (Table 2) is impossible because a feature-classified galaxy can have multiple features, while a class-classified galaxy belongs to only one class.

In our opinion, it is more efficient to use the existing catalogs of galaxies (for example, elliptical, spiral, irregular, flat, gravitational lenses, mergers, etc.) as training ones to determine the morphological types of galaxies. Binning these catalogs by redshift, we can sequentially create new morphological catalogs at

Table 4. **Comparison of classifications of the studied SDSS DR9 galaxies by the CNN model into five morphological classes [54] and by three photometry-based methods: multi-parametric diagram (MPD) into elliptical, spiral, and irregular galaxies [58, 60]; machine learning with Random Forest (RF) and Support Vector machine (SVM) into early and late morphological types [55, 70]. The number of only those galaxies, N gal, that have the best threshold probability of belonging to one or another morphological class is pointed out**

Photometry-based	*N* gal	Type	Image-based, CNN, classes				
			Completely round	Round in between	Cigar-shaped	Edge-on	Spiral
MPD, $N = 308466$	138947	E	35389	65839	14360	12067	11292
	110454	Sp	13645	41047	12803	6065	36894
	59065	Irr	7627	20658	4224	2108	24448
RF, $N = 308466$	131663	Early	36424	66043	12268	8549	8379
	176803	Late	20237	61501	19119	11691	64255
SVM, $N = 308466$	131099	Early	36135	65646	12477	8790	8051
	177367	Late	20526	61898	18910	11450	64583

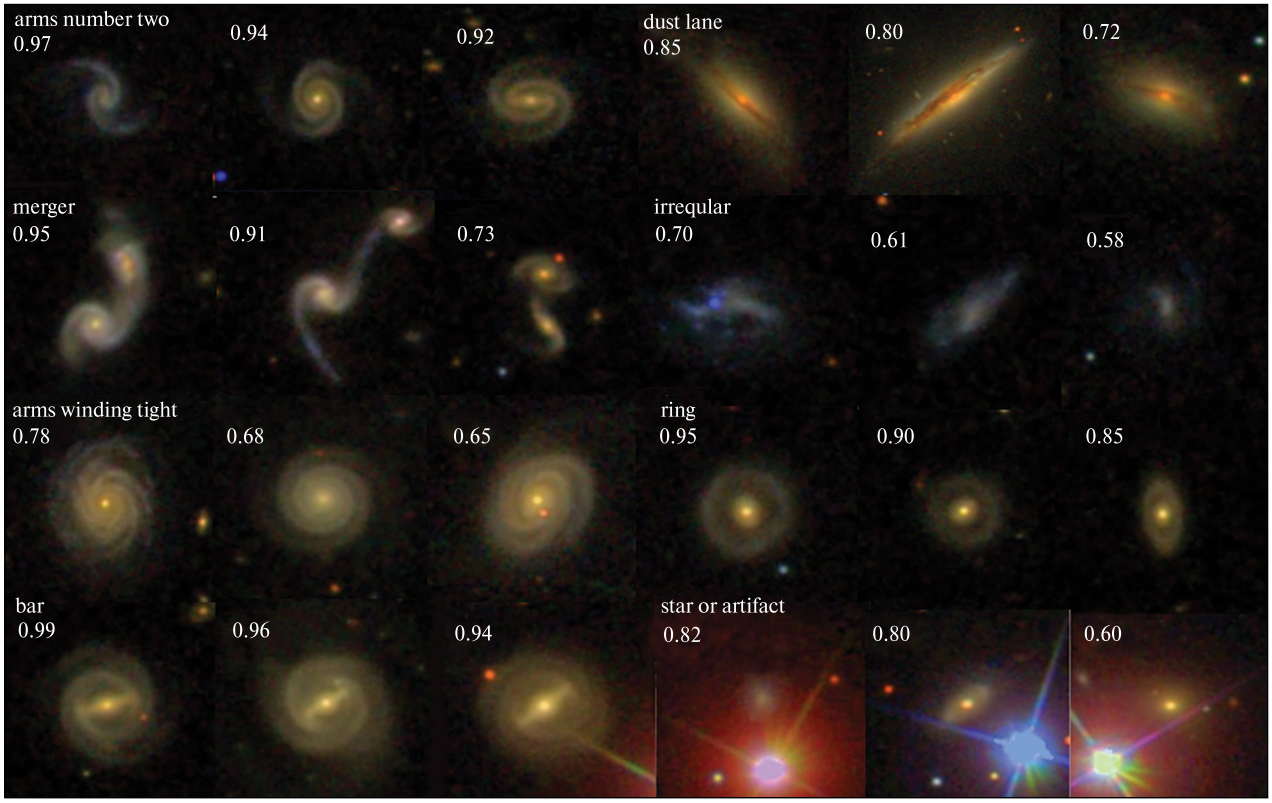

Figure 8. The examples of galaxies with some morphological features (bar, ring, irregular, merger, dust lane, arms winding tight, arms number 2, and star or artifact) from the inference SDSS data set with their two nearest neighbors from the GZ2 training data set

higher redshifts and, after a thorough check, ~~to~~ use new catalogs as training, etc. The emergence of new data on galaxy images for more in-depth samples by future observatories will provide such an algorithm by the data for CNN models. Meanwhile, it is useful to use both photometry- and image-based methods. Our approach to transferring the annotated classification of galaxies to fainter and smaller galaxies using adversarial validation with train-test splitting and image sizing is in favor of the correct applicability of the CNN classifier and the efficiency of the algorithm.

4.4. ***CNN classification by the detailed galaxy morphological features.*** The quality of inference morphological features from the test data sets of galaxies is summarized in Table 2 and Table 3. Our CNN model for the classification of galaxies by their detailed structural morphology gives accuracy in the range of 83.3...99.4 % depending on 32 features (exception is for "disturbed" (68.55 %) and "arms winding medium" (77.39 %), the number of galaxies with the given feature in the inference data set, the galaxy image quality (Table 2 and Table 3). To reach it, we calculated the number of galaxies that passed the selected threshold for the acceptance of detailed morphological features. The examples of classification on inference galaxy data set are given in Fig. 8. As a result, for the first time, we assigned the detailed morphological classification for more than 140 000 low-redshift galaxies with $m_r < 17.7$ from the SDSS DR9, which has the highest adversarial score by the CNN classifier.

Using the adversarial validation technique, we managed the optimal train-test split of galaxies from the training data set to verify our CNN model based on the DenseNet-201 realistically. We have also found optimal galaxy image transformations, which help to increase the classifier's generalization ability as it

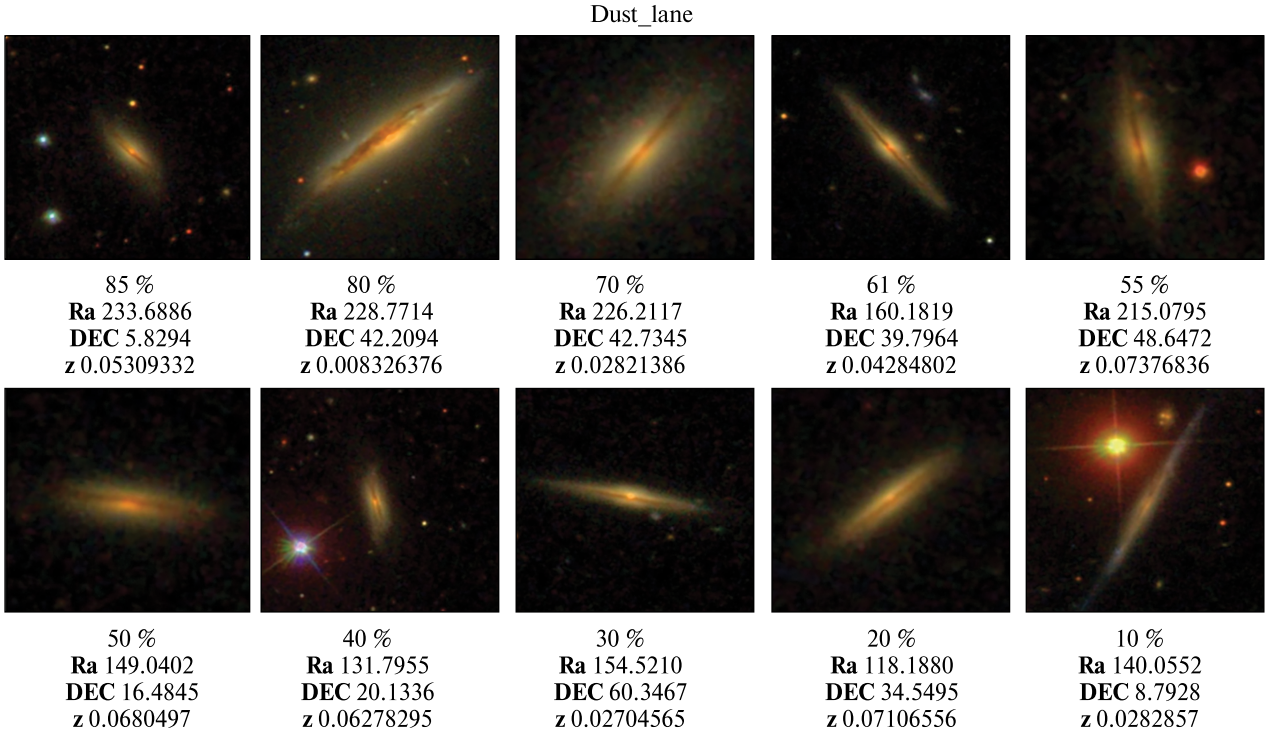

Figure 9: Examples of galaxies labeled as "dust lane". In the caption below each image: CNN probability to have this feature, RA and DEC, redshift

was tested with a specifically created test data set. We can compare our results with the work by Dieleman et al. [82]. Namely, a level of agreement and model confidence presented in Fig. 9 of their paper demonstrates that classification overall accuracy for the analyzed examples is in the range of 82.52...96.04 % in dependence on the galaxy feature (the exception is for "no of arms", "arm tightness", "odd", and "bulge", where accuracy is less than 80 %). Exploiting similar augmentation procedures for the SDSS galaxy images, our approach was slightly different: in the choice of image data as the PNG files restricted for three *gri* bands as well as performing a multi-label task for detailed morphological classification, when the galaxy can be attributed with several features (for, example, labeling as "spiral", the galaxy can be also with "bar", "bulge" or "ring" and be characterized by a certain number of "arms").

Good train-test sampling mobility for the CNN classifier resulted in the catalogs of low-redshift galaxies with morphological features, which are supplements to this paper. The highest score (97...99 %) was attained for such features as a ring, irregular shape, bulge, star or artifact, edge-on, and dust lane.

So, we can underline that the train/test split has very important consequences because with its use, the CNN's applicability to the future LSST, WFIRST, and Euclid big data surveys will not depend on the need for a large training set of real data.

In general, this allows us to make a quick selection of galaxies with certain features for their subsequent analysis (see Table 2 and Table 3). Using the SDSS Navigate, we performed a preliminary visual inspection of samples of galaxies with such features as "dust lane, irregular, edge-on yes, ring, bar, merger, star or artifact" in order to reveal CNN efficiency to classify images from an astronomical point of view.

All the inspected galaxies labeled as "dust lane", "irregular", and "edge-on yes" demonstrate the perfect annotation. All these galaxies possess these features even having a lower probability by the CNN classifier (see examples in Fig. 9—11: "dust lane" in all range of probabilities, "irregular" till 30 %, "edge-on yes" till 60 %.

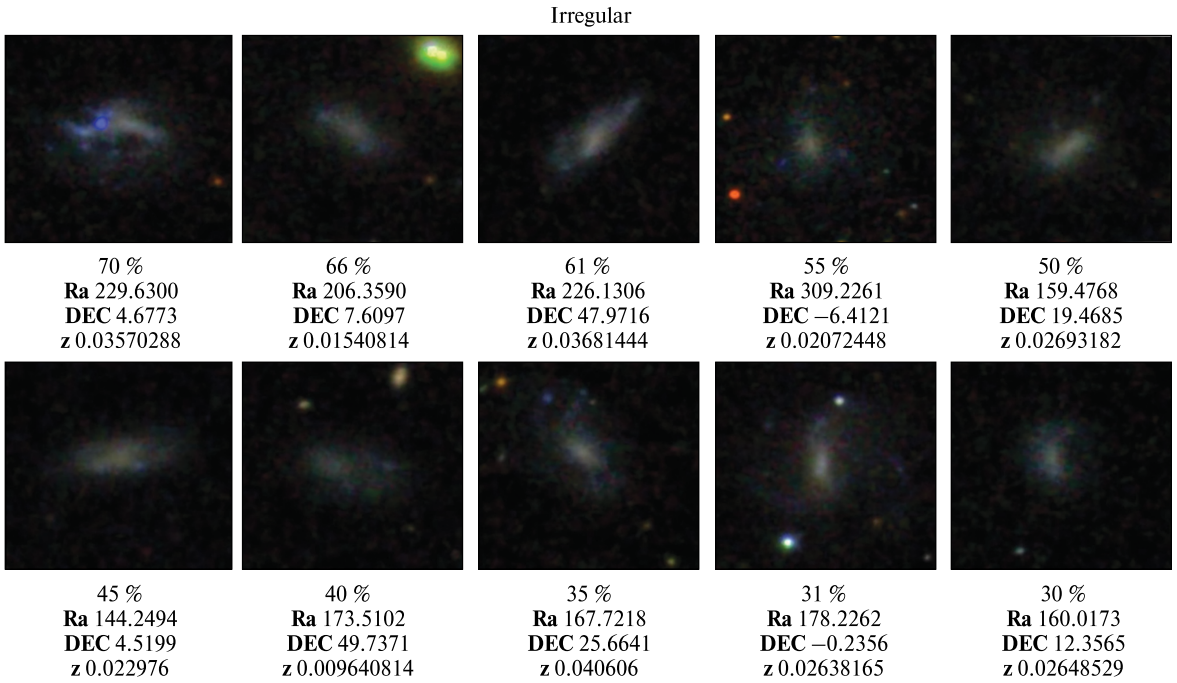

Figure 10: Examples of galaxies labeled as "irregular". In the caption below each image: CNN probability to have this feature, RA and DEC, redshift

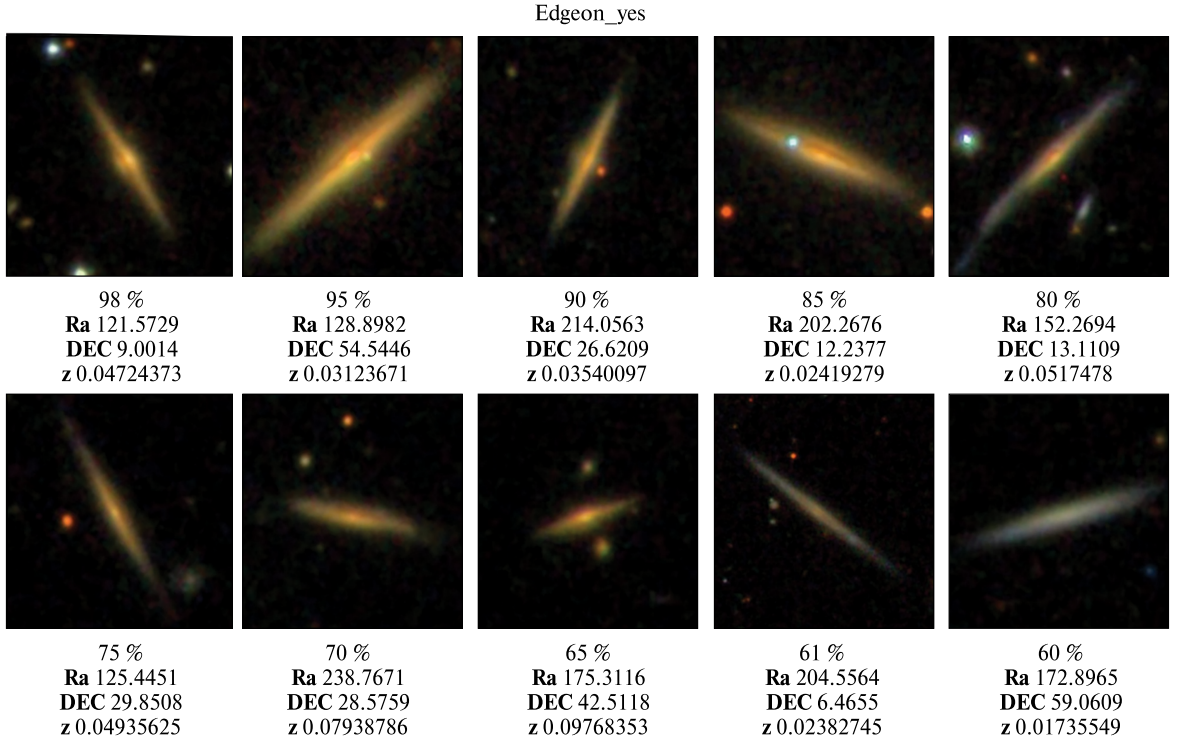

Figure 11: Examples of galaxies labeled as "edge-on yes". In the caption below each image: CNN probability to have this feature, RA and DEC, redshift

4.5. ***Notes on problem points of CNN image-based galaxy classification by their features.*** The evolutionary galaxy properties can affect ML methods' accuracy based on galaxies' photometry/image features. Among these misclassified types are the bluer HI-rich galaxies of early type and the redder HI-poor spiral galaxies; edge-on and galaxies seen face-on, especially with a pronounced bulge; the bulge-less (ultra-flat) galaxies with inclination 87°...90° for seen edge-on and 10°...0° for seen face-on. The face-on bulge-less galaxies can be considered counterparts to the edge-on disk galaxies giving additional information on their physical parameters, including photometry [54, 123]. So, their correct classification is very useful when compiling catalogs with a bulge to super-thin galaxies [124, 125] or studying the influence of the environment on the morphology and quenching of galaxies in dense environments (for example, [126] for the Hydra cluster). In such cases, where the surface brightness profile, color, and concentration indexes are needed, the ML algorithms trained over SDSS photometric parameters are less biased than when trained using GZ visual morphology (see, amongst others [54, 82, 115, 120, 127]).

At the same time, the results of applying the deep CNN to the images of our studied set [65, 66] with the aim of binary morphological classification (late and early types) have shown limitations. Namely, DL methods can classify rounded galaxy images as ellipticals. Still, it cannot catch the SED properties of galaxies more clearly than the Support Vector Machine trained on the photometric features of galaxies. To avoid several of these misclassifications, Lingard et al. [128] developed a novel method, Galaxy Zoo Builder, working well with face-on galaxy image modeling based on the four-component photometric decomposition of spiral galaxies. Earlier, Schawinski et al. [129] exploited the SDSS, GALEX, and GZ data to substantiate the transformation from disk to elliptical morphology of low-redshift galaxies.

Our visual inspection revealed a few more typical nuances about misclassified galaxy images.

As related to the galaxies with the "ring" feature, we note that such galaxies were correctly labeled in all the range of probabilities. But there are misclassified images, mostly at the higher redshifts, which are a) the disk galaxies with a bright bulge, b) galaxies with complicated contrast gradient of brightness (see Fig. 12, two last images) as well as c) elliptical galaxies with a bright core, in which the brightness is not distributed smoothly towards the periphery, d) merging galaxies with a bright core and outer component distinctly differed in brightness, as a result, the neural network considers the outer component to be a ring.

The creation of the representative catalog of galaxies with ring(s) could be very useful ([130, 131]). For example, Smirnov and Reshetnikov [131] collected the samples of polar- and collision- ring galaxies from all the published data in several deep fields. Doing this painstaking preliminary search, they constructed the luminosity function for the ringed galaxies and confirmed the increase in their volume density with redshift: up to $z \sim 1$ their density grows as $(1 + z)^m$, where $m \geq 5$. As related to the problem point of elliptical galaxies with the bright core, we link to the paper by Tarsitano et al. [107], who developed a promising CNN approach based on the training of elliptical isophotes in the light distribution.

The galaxy images labeled with "bar" have typical misclassifications. It has been happening when a) a central part of spiral arms of the edge-on galaxy is classified as a bar, b) the nuclei of merging galaxies are visually located near one another, then the CNN matches this as a bar. The samples of misclassified images with the "bar" feature are in Fig. 13. Bhambra et al. [85] proposed the explainable artificial intelligence (XAI) techniques to measure galactic bar lengths and bulge-to-disk ratio. They used the Hoyle bar length catalog [132] vs. GZ annotated data and demonstrated that XAI works more successfully in predictions of a bar feature. Also, taking into account the class of "smooth" galaxies (no bar, spiral arms, or other structure presents), these authors demonstrate the difficulties in reconciling differences between the ML model predictions and the GZ consensus. We agree with their conclusion that the citizen science method of classifying galaxies is less easily explained than ML methods.

We will not analyze the galaxy samples related to the "spiral arms number" features. This task is perfectly studied by Hart et al. [106]. Their method allowed them to overcome where the rarer many-armed samples were incomplete, and the two-armed category suffered from sample contamination. They

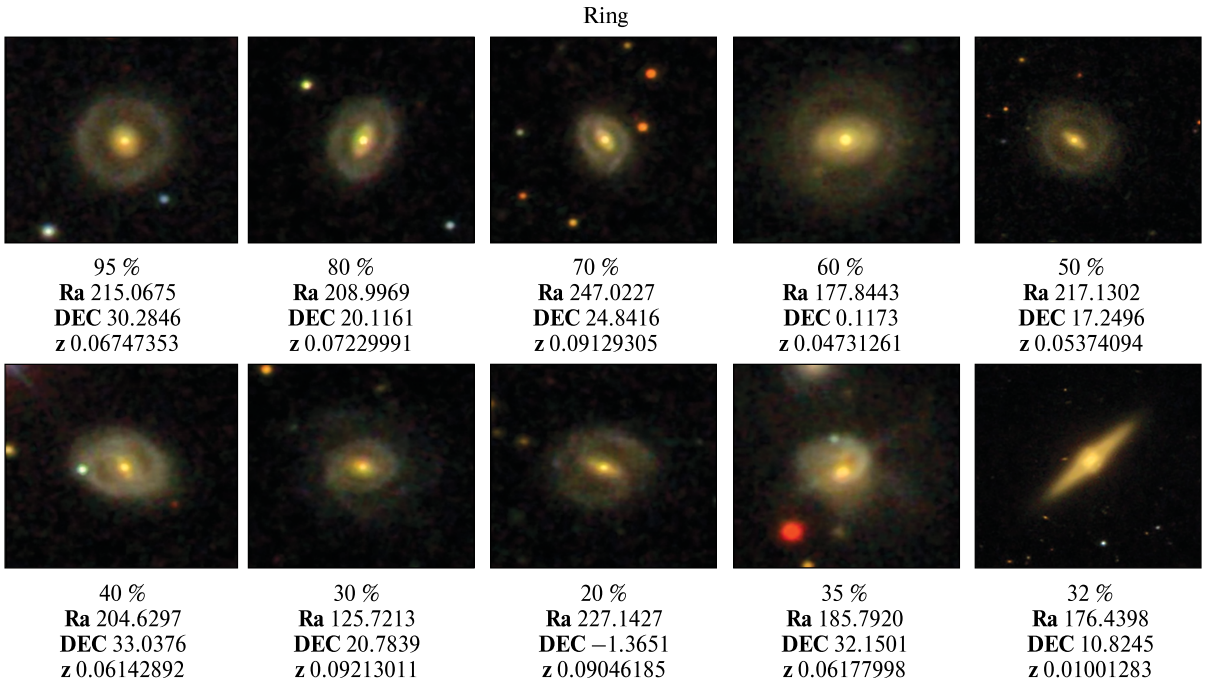

Figure 12: Examples of galaxies labeled as a "ring". In the caption below each image: CNN probability to have this feature, RA and DEC, redshift

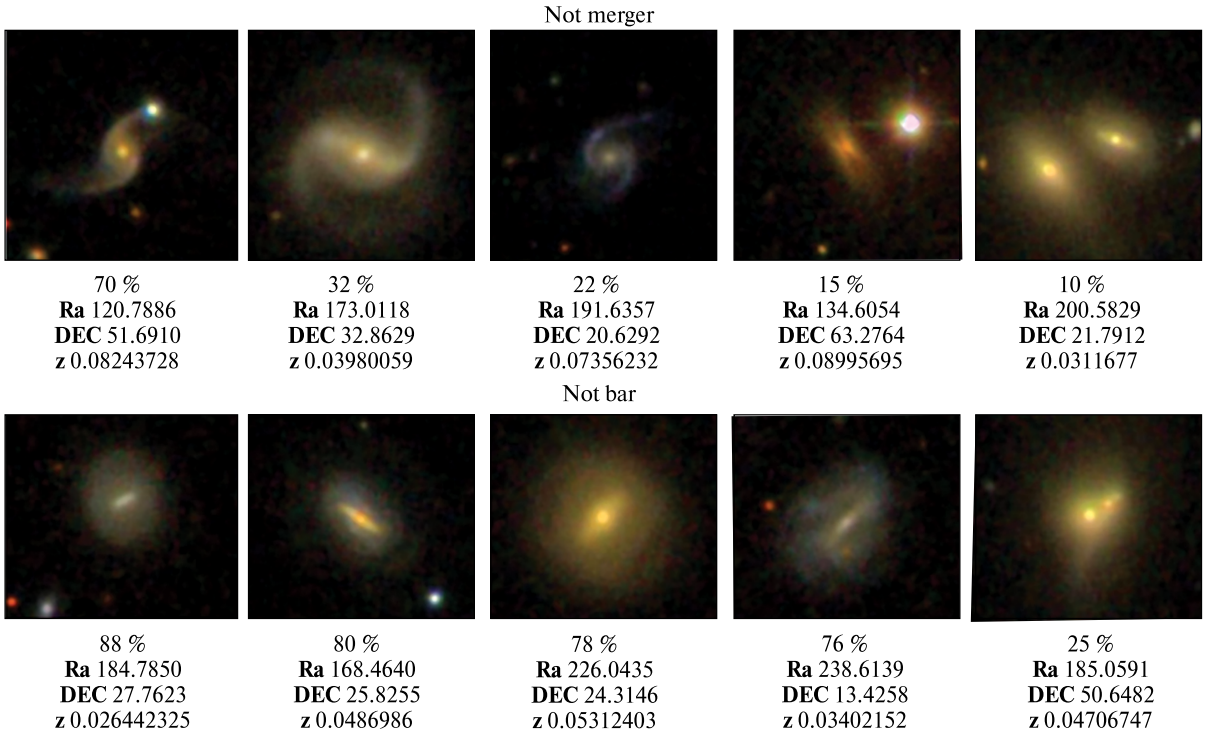

Figure 13: Examples of misclassified images of galaxies: with "merger" and "bar" features. In the caption below each image: CNN probability to have this feature, RA and DEC, redshift

created a sample of about 18000 SDSS DR7 galaxies at $0.03 < z < 0.08$ with $M_r < -21$, which was sorted by arm multiplicity and further studied for star-forming activity.

All the galaxy images with the "star or artifacts" have these features. All of them contain galaxies that are classified. Bright stars and/or artifacts that obscure the image of a galaxy lead to misclassification of galaxies in most cases.

The sample of "merger" galaxies also has false images, when a) galaxies are the optical pair, b) the star falls into the image background near a spiral galaxy, then the CNN considers the star as an elliptical galaxy and keeps it as merging, c) spiral galaxies without interaction, but their arms are untwisted (see, examples, in Fig. 13). It is interesting to compare our results on merging galaxies with work by Reza [133], who also used the SDSS data and obtained that ExtraTrees classifier outperforms Neural Network for this distinct type of objects. It was noted that mergers are easily confused with both ellipticals and spirals when image-based classification is conducted. Our results are useful when compiling the catalogs of merging galaxies [104, 134—137].

As one can see, the CNN confident model predictions are highly accurate and allow us to filter big data collections of galaxy images with various morphological features. We expertized our obtained data and described several challenging images. When we develop the classification model, the aim is not only the state-of-the-art accuracy values but also defining problem points of the CNN model in working with galaxy images and training it to classify large surveys of galaxies no worse than an expert for small samples.

5. CONCLUSIONS

The image-based CNN classifier was exploited by us to create a morphological catalog of 315776 SDSS DR9 low-redshift galaxies ($z < 0.1$) following our previous works ([54, 55, 69]). This target data set of the SDSS galaxies is tightly overlapped with the annotated data from GZ2 [71]. For this reason, we divided it into two data sets: "inference", which does not match the GZ2 galaxies, and "training", which matches the GZ2 galaxies. In the presence of a pronounced difference of visual parameters between galaxies from the GZ2 training data set and galaxies without known morphological parameters, we applied novel procedures, which allowed us to get rid of this difference, especially for smaller and fainter SDSS galaxies with $m_r < 17.7$ from the inference data set. We describe in this paper how we applied the adversarial validation technique and managed the optimal train-test split of galaxies from the training data set to verify our CNN model based on the DenseNet-201 realistically. We have also found optimal galaxy image transformations, which help increase the classifier's generalization ability in similarity search, as is provided with a specifically created test data set.

We demonstrate for the first time that implication of the CNN model with the train-test split of data sets and size-changing function simulating a decrease in magnitude and size (data augmentation) significantly improves the classification of smaller and fainter SDSS galaxies. It can be considered as another way to improve the human bias for those galaxy images that had a poor vote classification in the GZ project. Such an approach, like autoimmunization, when the CNN classifier trained on very good images is able to retrain bad images from the same homogeneous sample, can be considered co-planar to other methods of combating such a human bias.

The most interesting data products with this approach were obtained for galaxy classification by 34 detailed morphology features. The accuracy of the CNN classifier is in the range of 83.3...99.4 % depending on 32 features (exception is for "disturbed" (68.55 %) and "arms winding medium" (77.39 %) features), the number of galaxies with the given feature in the inference data set, and the galaxy image quality (Table 2 and Table 3). To reach it, we calculated the number of galaxies that passed the best threshold for the acceptance of detailed morphological features. As a result, for the first time, we assigned the detailed morphological classification for more than 140000 low-redshift galaxies with $m_r < 17.7$ from the SDSS DR9 (inference data set), which has the highest adversarial score by the CNN classifier. The morphological catalogs of low-redshift SDSS galaxies with the most interesting features are available through the UkrVO website http://ukr-vo.org/starcats/galaxies/ and will be supplemented to this paper through VizieR, as well as the catalog of galaxies with top five detailed morphological features (to

wit, with a maximal prediction probability to possess such a feature).

A visual inspection of the samples of galaxies with certain morphological features allowed us to reveal typical problem points of galaxy image classification by shape and features from the astronomical point of view. We analyzed them in the discussion section, where we also compare machine learning photometry- and image- based approaches testifying that the best results are being performed with all of the galaxy data types (photometry, image, spectroscopy). We believe our results and notes on problem points will be useful to strengthen the CNN applicability and help in the morphological classification of galaxies within the current and forthcoming deep sky surveys at the petabyte scale.

Acknowledgements. We thank Prof. Massimo Capacciolli and Dr. Valentina Karachentseva for the helpful discussion and remarks. The authors are deeply grateful to both referees for a detailed review of the article, their questions, comments, and suggestions, which significantly improved the presentation of our results.

This paper uses data generated via the Zooniverse.org platform, the development of which is funded by generous support including a Global Impact Award from Google and a grant from the Alfred P. Sloan Foundation. This publication has been made possible by the participation of hundreds of thousands of volunteers in the Galaxy Zoo project. We thank the Galaxy Zoo team. The use of the SDSS [138, 139] and SAO/NASA Astrophysics Data System was extensively applicable. This study has also been made with NASA/IPAC Extragalactic Database (NED), which is operated by the Jet Propulsion Laboratory, California Institute of Technology, under contract with the NASA. This research has made use of the SIMBAD database, operated at CDS, Strasbourg, France [140].

This work was done in the frame of the Program of the NAS of Ukraine "Support for the development of priority fields of scientific research" and the Target Program of Space Science Research of the NAS of Ukraine. I. B. Vavilova thanks the Wolfgang Pauli Institute, Vienna, Austria, for the support in the frame of "The Pauli Ukraine Project" (2022) under the "Models in plasma, Earth and space science" program.

REFERENCES

1. Agnello A., Kelly B. C., Treu T., Marshall P. J. (2015). Data mining for gravitationally lensed quasars. *Mon. Notic. Roy. Astron. Soc.*, **448** (2), 1446—1462. doi:10.1093/mnras/stv037.
2. Ostrovski F., McMahon R. G., Connolly A. J., et al. (2017). VDES J2325-5229 a z = 2.7 gravitationally lensed quasar discovered using morphology-independent supervised machine learning. *Mon. Notic. Roy. Astron. Soc.*, **465** (4), 4325—4334. doi:10.1093/mnras/stw2958.
3. Lanusse F., Ma Q., Li N., et al. (2018). CMU DeepLens: deep learning for automatic image based galaxy-galaxy strong lens finding. *Mon. Notic. Roy. Astron. Soc.*, **473** (3), 3895—3906. doi:10.1093/mnras/stx1665.
4. Jacobs C., Collett T., Glazebrook K., et al. (2019). Finding highredshift strong lenses in DES using convolutional neural networks. *Mon. Notic. Roy. Astron. Soc.*, **484** (4), 5330—5349. doi:10.1093/mnras/stz272.
5. Khramtsov V., Sergeyev A., Spiniello C., et al. (2019). Kids-squad - ii. machine learning selection of bright extragalactic objects to search for new gravitationally lensed quasars. *Astron. and Astrophys.*, **A632**, A56. doi:10.1051/0004-6361/201936006.
6. Petrillo C. E., Tortora C., Chatterjee S., et al. (2019). Testing convolutional neural networks for finding strong gravitational lenses in KiDS. *Mon. Notic. Roy. Astron. Soc.*, **482** (1), 807—820. doi:10.1093/mnras/sty2683.
7. Ribli D., Pataki B. A., Zorrilla Matilla J. M., et al. (2019). Weak lensing cosmology with convolutional neural networks on noisy data. *Mon. Notic. Roy. Astron. Soc.*, **490** (2), 1843—1860. doi:10.1093/mnras/stz2610.
8. Pourrahmani M., Nayyeri H., Cooray A. (2018). LensFlow: A Convolutional Neural Network in Search of Strong Gravitational Lenses. *Astrophys. J.*, **856** (1), 68. doi:10.3847/1538-4357/aaae6a.
9. Pasquet J., Bertin E., Treyer M., et al. (2019). Photometric redshifts from SDSS images using a convolutional neural network. *Astron. and Astrophys.*, **621**, A26. doi:10.1051/0004-6361/201833617.
10. Fussell L., Moews B. (2019). Forging new worlds: high-resolution synthetic galaxies with chained generative a dversarial networks. *Mon. Notic. Roy. Astron. Soc.*, **485** (3), 3203—3214. doi:10.1093/mnras/stz602.
11. Salvato M., Ilbert O., Hoyle B. (2019). The many flavours of photometric redshifts. *Nature Astron.*, **3**, 212—222. doi:10.1038/s41550-018-0478-0.

12. Bonnett C., Troxel M. A., Hartley W., et al. (2016). Redshift distributions of galaxies in the Dark Energy Survey Science Verification shear catalogue and implications for weak lensing. *Phys. Rev. D*, **94** (4), 042005. doi:10.1103/PhysRevD.94.042005.
13. Amaro V., Cavuoti S., Brescia M., et al. (2019). Statistical analysis of probability density functions for photometric redshifts through the KiDS-ESO-DR3 galaxies. *Mon. Notic. Roy. Astron. Soc.*, **482** (3), 3116—3134. doi:10.1093/mnras/sty2922.
14. Sadeh I., Abdalla F. B., Lahav O. (2016). ANNz2: Photometric Redshift and Probability Distribution Function Estimation using Machine Learning. *Publ. ASP*, **128** (968), 104502. doi:10.1088/1538-3873/128/968/104502.
15. Pasquet-Itam J., Pasquet J. (2018). Deep learning approach for classifying, detecting and predicting photometric redshifts of quasars in the Sloan Digital Sky Survey stripe 82. *Astron. and Astrophys.*, **611**, A97. doi:10.1051/0004-6361/201731106.
16. Kügler S. D., Gianniotis N. (2016). Modelling multimodal photometric redshift regression with noisy observations. arXiv:1607.06059.
17. Speagle J. S., Eisenstein D. J. (2017). Deriving photometric redshifts using fuzzy archetypes and self-organizing maps - II. Implementation. *Mon. Notic. Roy. Astron. Soc.*, **469** (1), 1205—1224. doi:10.1093/mnras/stx510.
18. D'Isanto A., Cavuoti S., Gieseke F., Polsterer K. L. (2018). Return of the features. Efficient feature selection and interpretation for photometric redshifts. *Astron. and Astrophys.*, **616**, A97. doi:10.1051/0004-6361/201833103.
19. Elyiv A. A., Melnyk O. V., Vavilova I. B., et al. (2020). Machine-learning computation of distance modulus for local Galaxies. *Astron. and Astrophys.*, **635**. A124. doi:10.1051/0004-6361/201936883.
20. Rastegarnia F., Mirtorabi M. T., Moradi R., et al. (2022). Deep learning in searching the spectroscopic redshift of quasars. *Mon. Notic. Roy. Astron. Soc.*, **511** (3), 4490—4499. doi:10.1093/mnras/stac076.
21. Elyiv A. A., Karachentsev I. D., Karachentseva V. E., et al. (2013). Low-density structures in the Local Universe. II. Nearby cosmic voids. *Astrophys. Bull.*, **68** (1), 1—13. doi:10.1134/S199034131301001X.
22. Koulouridis E., Plionis M., Melnyk O., Elyiv A., et al. (2014). X-ray AGN in the XMMLSS galaxy clusters: no evidence of AGN suppression. *Astron. and Astrophys.*, **567**, A83. doi:10.1051/0004-6361/201423601.
23. Elyiv A., Marulli F., Pollina G., et al. (2015). Cosmic voids detection without density measurements. *Mon. Notic. Roy. Astron. Soc.*, **448** (1), 642—653. doi:10.1093/mnras/stv043.
24. Schawinski K., Zhang C., Zhang H., et al. (2017). Generative adversarial networks recover features in astrophysical images of galaxies beyond the deconvolution limit. *Mon. Notic. Roy. Astron. Soc.*, **467** (1), L110—L114. doi:10.1093/mnrasl/slx008.
25. Vavilova I. B., Elyiv A. A., Vasylenko M. Y. (2018). Behind the zone of avoidance of the Milky Way: What can we restore by direct and indirect methods? *Russian Radio Phys. and Radio Astron.,* **23** (4), 244—257. doi:10.15407/rpra23.04.244.
26. Rodríguez A. C., Kacprzak T., Lucchi A., et al. (2018). Fast cosmic web simulations with generative adversarial networks. *Comput. Astrophys. Cosmol.*, **5** (1), 4. doi:10.1186/s40668-018-0026-4.
27. Khramtsov V., Akhmetov V., Fedorov P. (2020). The Northern Extragalactic WISE × Pan-STARRS (NEWS) catalogue. Machine-learning identification of 40 million extragalactic objects. *Astron. and Astrophys.*, **644**, A69. doi: 10.1051/0004-6361/201834122.
28. Hong S. E., Jeong D., Hwang H. S., Kim J. (2021). Revealing the local cosmic web from galaxies by deep learning. *Astrophys. J.*, **913** (1), 76. doi:10.3847/1538-4357/abf040.
29. Khramtsov V., Spiniello C., Agnello A., Sergeyev A. (2021). VEXAS: VISTA EXtension to Auxiliary Surveys. Data Release 2: Machine-learning based classification of sources in the Southern Hemisphere. *Astron. and Astrophys.*, **651**, A69. doi:10.1051/0004-6361/202040131.
30. Diakogiannis F. I., Lewis G. F., Ibata R. A., et al. (2019). Reliable mass calculation in spherical gravitating systems. *Mon. Notic. Roy. Astron. Soc.*, **482** (3), 3356—3372. doi:10.1093/mnras/sty2931.
31. Tsizh M., Novosyadlyj B., Holovatch Y., Libeskind N. I. (2020). Large-scale structures in the CDM Universe: network analysis and machine learning. *Mon. Notic. Roy. Astron. Soc.*, **495** (1), 1311—1320. doi:10.1093/mnras/staa1030.
32. Chen Y., Mo H. J., Li C., et al. (2020). Relating the Structure of Dark Matter Halos to Their Assembly and Environment. *Astrophys. J.*, **899** (1), 81. doi:10.3847/1538-4357/aba597.
33. Moriwaki K., Shirasaki M., Yoshida N. (2021). Deep learning for line intensity mapping observations: Information extraction from noisy maps. *Astrophys. J. Lett.*, **906** (1), L1. doi:10.3847/2041-8213/abd17f.
34. Flamary R. (2016). Astronomical image reconstruction with convolutional neural networks. arXiv:1612.04526.
35. Kremer J., Stensbo-Smidt K., Gieseke F., et al. (2017). *Big Universe, Big Data: Machine Learning and Image Analysis for Astronomy*. arXiv:1704.04650.
36. Savanevych V. E., Khlamov S. V., Vavilova I. B., et al. (2018). A method of immediate detection of objects with a near-zero apparent motion in series of CCD-frames. *Astron. and Astrophys.*, **609**, A54. doi:10.1051/0004-6361/201630323.
37. Villarroel B., Soodla J., Comerón S., et al. (2020). The vanishing and appearing sources during a century of observations project. I. USNO objects missing in modern sky surveys and follow-up observations of a "Missing Star". *Astron. J.,* **159** (8), 19. doi:10.3847/1538-3881/ab570f.

38. Pavlenko Y., Kulyk I., Shubina O., et al. (2022). New exocomets of β Pic. *Astron. and Astrophys.*, **660**, A49. doi:10.1051/0004-6361/202142111.
39. Reiman D. M., Göhre B. E. (2019). Deblending galaxy superpositions with branched generative adversarial networks. *Mon. Notic. Roy. Astron. Soc.*, **485** (2), 2617—2627. doi:10.1093/mnras/stz575.
40. Buchanan J. J., Schneider M. D., Armstrong R. E., et al. (2021). *Gaussian process classification for galaxy blend identification in LSST*. arXiv: 2107.09246.
41. El Bouchefry K., de Souza R. S. (2020). *Learning in big data: Introduction to machine learning*. Knowledge Discovery in Big Data from Astronomy and Earth Observation. Eds P. Škoda, F. Adam, 225—249. doi:10.1016/B978-0-12-819154-5.00023-0.
42. Burgazli A., Sergijenko O., Vavilova I. (2022). *Machine learning in cosmology and gravitational wave astronomy: recent trends*. Horizons in Computer Science Research. Ed. T. S. Clary. New York: Nova Sci. Publ. Inc., Vol. 22, Chapter 7, 193—240.
43. Kang S.-J., Fan J.H., Mao W., et al. (2019). Evaluating the optical classification of Fermi BCUs using machine learning. *Astrophys. J.*, **872** (2), 189. arXiv:1902.07717. doi:10.3847/1538-4357/ab0383.
44. Krause M., Pueschel E., Maier G. (2017). Improved γ/hadron separation for the detection of faint γ-ray sources using boosted decision trees. *Astropart. Phys.*, **89**, 1—9. doi:10.1016/j.astropartphys.2017.01.004.
45. Ruhe T. (2020). Application of machine learning algorithms in imaging Cherenkov and neutrino astronomy. *Int. J. Mod. Phys. A*, **35** (33), 2043004-778. doi:10.1142/S0217751X20430046.
46. Morello G., Morris P. W., Van Dyk S. D., et al. (2018). Applications of machine-learning algorithms for infrared colour selection of Galactic Wolf-Rayet stars. *Mon. Notic. Roy. Astron. Soc.*, **473** (2), 2565—2574. doi:10.1093/mnras/stx2474.
47. Ciuca R., Hernández O. F. (2017). A Bayesian framework for cosmic string searches in CMB maps. *J. Cosm. Astropart. Phys.*, **2017** (8), 028. doi:10.1088/1475-7516/2017/08/028.
48. Aniyan A. K., Thorat K. (2017). Classifying radio galaxies with the convolutional neural network. *Astrophys. J. Suppl.*, **230** (2), 20. doi:10.3847/1538-4365/aa7333.
49. Lukic V., Brüggen M., Banfield J. K., et al. (2018). Radio galaxy Zoo: Compact and extended radio source classification with deep learning. *Mon. Notic. Roy. Astron. Soc.*, **476** (1), 246—260. doi:10.1093/mnras/sty163.
50. Ma Z., Xu H., Zhu J., et al. (2019). A machine learning based morphological classification of 14,245 radio AGNs selected from the Best-Heckman sample. *Astrophys. J. Suppl.*, **240** (2), 34. doi:10.3847/1538-4365/aaf9a2.
51. Scaife A. M. M., Porter F. (2021). Fanaroff-Riley classification of radio galaxies using group-equivariant convolutional neural networks. *Mon. Notic. Roy. Astron. Soc.*, **503** (2), 2369—2379. doi:10.1093/mnras/stab530.
52. Ciprijanović A., Kafkes D., Downey K., et al. (2021). DeepMerge. II. Building robust deep learning algorithms for merging galaxy identification across domains. *Mon. Notic. Roy. Astron. Soc.*, **506** (1), 677—691. doi:10.1093/mnras/stab1677.
53. Shamir L. (2021). Automatic identification of outliers in Hubble Space Telescope galaxy images. *Mon. Notic. Roy. Astron. Soc.*, **501** (4), 5229—5238. doi:10.1093/mnras/staa4036.
54. Vavilova I. B., Dobrycheva D. V., Vasylenko M. Y., et al. (2021). Machine learning technique for morphological classification of galaxies from the SDSS. I. Photometry-based approach. *Astron. and Astrophys.*, **648,** A122. doi:10.1051/0004-6361/ 202038981.
55. Vavilova I. B., Khramtsov V., Dobrycheva D. V., et al. (2022). Machine learning technique for morphological classification of galaxies from SDSS. II. The image-based morphological catalogs of galaxies at $0.02 < z < 0.1$. *Space Sci. & Technol.*, **28** (1), 3—22. doi:10.15407/knit2022.01.003.
56. Walmsley M., Smith L., Lintott C., et al. (2020). Galaxy Zoo: probabilistic morphology through Bayesian CNNs and active learning. *Mon. Notic. Roy. Astron. Soc.*, **491** (2), 1554—1574. doi:10.1093/mnras/stz2816.
57. Muller A., Guido S. (2016). *Introduction to Machine Learning with Python*. O'Reilly Media.
58. Melnyk O. V., Dobrycheva D. V., Vavilova I. B. (2012). Morphology and color indices of galaxies in Pairs: Criteria for the classification of galaxies. *Astrophys.*, **55** (3), 293—305. doi:10.1007/s10511-012-9236-7.
59. Dobrycheva D. V., Melnyk O. V., Vavilova I. B., Elyiv A. A. (2014). Environmental properties of galaxies at $z < 0.1$ from the SDSS via the Voronoi tessellation. *Odessa Astron. Publ.*, **27**, 26.
60. Dobrycheva D. V., Melnyk O. V., Vavilova I. B., Elyiv A. A. (2015). Environmental density vs. colour indices of the low redshifts galaxies. *Astrophys.*, **58** (2), 168—180. doi:10.1007/s10511-015-9373-x.
61. Dobrycheva D. V., Vavilova I. B., Melnyk O. V., Elyiv A. A. (2017). *Machine learning technique for morphological classification of galaxies at $z \le 0.1$ from the SDSS*. arXiv:1712.08955.
62. Dobrycheva D. V. (2017). *Morphological content and color indices bimodality of a new galaxy sample at the redshifts $z < 0.1$*: Ph.D. thesis. Kyiv: MAO of the NAS of Ukraine.
63. Dobrycheva D. V., Vavilova I. B., Melnyk O. V., Elyiv A. A. (2018). Morphological Type and Color Indices of the SDSS DR9 Galaxies at $0.02 < z \le 0.06$. *Kinematics and Phys. Celestial Bodies*, **34** (6), 290—301. doi:10.3103/S0884591318060028.
64. Vasylenko M. Y., Dobrycheva D. V., Vavilova I. B., et al. (2019). Verification of Machine Learning Methods for Binary Morphological Classification of Galaxies from SDSS. *Odessa Astron. Publ.*, **32**, 46. doi:10.18524/1810-4215.2019.32.182538.

65. Khramtsov V., Dobrycheva D. V., Vasylenko M. Y., Akhmetov V. S. (2019). Deep learning for morphological classification of galaxies from SDSS. *Odessa Astron. Publ.*, **32**, 21. doi:10.18524/1810-4215.2019.32.182092.
66. Vasylenko M., Dobrycheva D., Khramtsov V., Vavilova I. (2020). Deep Convolutional Neural Networks models for the binary morphological classification of SDSS-galaxies. *Commun. BAO*, **67**, 354. doi:10.52526/25792776-2020.67.2-354.
67. Vavilova I., Dobrycheva D., Vasylenko M., et al. (2020). *Multiwavelength extragalactic surveys: Examples of data mining*. Knowledge Discovery in Big Data from Astronomy and Earth Observation. Eds. P. Skoda and F. Adam. Elsevier, Ch. 16, 307—323. doi:10.1016/B978-0-12-819154-5.00028-X.
68. Vavilova I., Elyiv A., Dobrycheva D., Melnyk O. (2021). T*he Voronoi tessellation method in astronomy*. Intelligent Astrophysics. Eds I. Zelinka, M. Brescia, D. Baron. Springer, Cham, **39** (3), 57—79. doi:10.1007/978-3-030-65867-0_3.
69. Vavilova I. B., Dobrycheva D. V., Vasylenko M. Y., et al. (2021). VizieR Online Data Catalog: SDSS galaxies morphological classification (Vavilova+, 2021), VizieR Online Data Catalog (2021) J/A+A/648/A122.
70. Vavilova I. B., Khramtsov V., Dobrycheva D. V., et al. VizieR Online Data Catalog: Galaxies at 0.02<z<0.1 morphological catalog (Vavilova+, 2022), VizieR Online Data Catalog (2022) J/other/KNIT/28.3/gal5mcls.
71. Willett K. W., Lintott C. J., Bamford S. P., et al. (2013). Galaxy Zoo 2: detailed morphological classifications for 304 122 galaxies from the Sloan Digital Sky Survey. *Mon. Notic. Roy. Astron. Soc.*, **435** (4), 2835—2860. doi:10.1093/mnras/stt1458.
72. Blanton M. R., Dalcanton J., Eisenstein D., et al. (2001). The luminosity function of galaxies in SDSS commissioning data. *Astron. J.*, **121** (5), 2358—2380. doi:10.1086/320405.
73. Yasuda N., Fukugita M.,. Narayanan V. K., et al. (2001). Galaxy Number Counts from the Sloan Digital Sky Survey Commissioning Data. *Astron. J.*, **122** (3), 1104—1124. doi:10.1086/322093.
74. Walmsley M., Lintott C., Geron T., et al. (2021). Galaxy ZOO DECaLSs: *Detailed visual morphology measurements from volunteers and deep learning for 314000 galaxies*. arXiv:2102.08414.
75. Lupton R., Blanton M. R., Fekete G., et al. (2004). Preparing red-green-blue images from CCD data. *Publ. ASP*, **116** (816), 133—137. doi:10.1086/382245.
76. Wang N., Choi J., Brand D., et al. (2018). *Training deep neural networks with 8-bit floating point numbers*. arXiv e-prints. arXiv:1812.08011.
77. Ren W., Yu Y., Zhang J., Huang K. (2014). *Learning convolutional nonlinear features for k nearest neighbor image classification*. 22nd Int. Conf. on Pattern Recognition, 4358—4363.
78. Honghui S. (2016). Galaxy classification with deep convolutional neural networks: Ph.D. thesis. University of Illinois at Urbana-Champaign.
79. Meyer B. J., Harwood B., Drummond T. (2018). *Deep metric learning and image classification with nearest neighbour Gaussian kernels.* 25th IEEE Int. Conf. on Image Processing, 151—155.
80. Pan J., Pham V., Dorairaj M., et al. (2020). *Adversarial validation approach to concept drift problem in user targeting automation systems at uber*. arXiv:2004.03045.
81. Bishop C. (1995). *Neural networks for pattern recognition*. Oxford: Univ. Press, USA.
82. Dieleman S., Willett K. W., Dambre J. (2015). Rotation-invariant convolutional neural networks for galaxy morphology prediction. *Mon. Notic. Roy. Astron. Soc.*, **450** (2), 1441—1459. doi:10.1093/mnras/stv632.
83. He K., Zhang X., Ren S., Sun J. (2015). *Deep residual learning for image recognition*. arXiv:1512.03385.
84. Vega-Ferrero J., Dominguez Sanchez H., Bernardi M., et al. (2021). Huertas-Company, Pushing automated morphological classifications to their limits with the Dark Energy Survey. *Mon. Notic. Roy. Astron. Soc.*, **506** (2), 1927—1943. doi:10.1093/mnras/stab594.
85. Bhambra P., Joachimi B., Lahav O. (2022). Explaining deep learning of galaxy morphology with saliency mapping. *Mon. Notic. Roy. Astron. Soc.*, **511** (4), 5032—5041. doi:10.1093/mnras/stac368.
86. Gupta R., Srijith P. K., Desai S. (2022). Galaxy morphology classification using neural ordinary differential equations. *Astron. Comp.*, **38**, 100543. doi:10.1016/j.ascom.2021.100543.
87. Huang G., Liu Z., van der Maaten L., Weinberger K. Q. (2018). *Densely connected convolutional networks*. arXiv:1608.06993.
88. Szegedy C., Vanhoucke V., Ioffe S., et al. (2015). *Rethinking the inception architecture for computer vision*. arXiv:1512.00567.
89. Szegedy C., Ioffe S., Vanhoucke V., Alemi A. (2016). *Inception-v4, inception resnet and the impact of residual connections on learning*. arXiv:1602.07261.
90. Zoph B., Vasudevan V., Shlens J. (2017). *Learning transferable architectures for scalable image recognition*. arXiv:1707.07012.
91. Simonyan K., Zisserman A. (2015). *Very deep convolutional networks for largescale image recognition*. arXiv:1409.1556.
92. Chollet F. (2017). *Xception: Deep learning with depthwise separable convolutions*. arXiv:1610.02357.
93. Bradley A. P. (1997). The use of the area under the ROC curve in the evaluation of machine learning algorithms. *Pattern Recognition*, **30** (7), 1145—1159. doi:10.1016/S0031-3203(96)00142-2.
94. Rahmani S., Teimoorinia H., Barmby P. (2018). Classifying galaxy spectra at 0.5<z<1 with self-organizing maps. *Mon. Notic. Roy. Astron. Soc.*, **478** (4), 4416—4432. doi:10.1093/mnras/sty1291.

95. Curti M., Hayden-Pawson C., Maiolino R., et al. (2022). What drives the scatter of local star-forming galaxies in the BPT diagrams? A Machine Learning based analysis. *Mon. Notic. Roy. Astron. Soc.*, **512** (3), 4136—4163. doi:10.1093/mnras/stac544.
96. Shi F., Liu Y-Y., Sun G.L., et al. A support vector machine for spectral classification of emission-line galaxies from the Sloan Digital Sky Survey. *Mon. Notic. Roy. Astron. Soc.*, **453** (1), 122—127. doi:10.1093/mnras/stv1617.
97. Tempel E., Saar E., Liivamägi L. J., et al. (2011). Galaxy morphology, luminosity, and environment in the SDSS DR7. *Astron. and Astrophys.*, **529** (2011) A53. doi:10.1051/0004-6361/201016196.
98. Tojeiro R., Masters K. L., Richards J., et al. (2013). The different star formation histories of blue and red spiral and elliptical galaxies. *Mon. Notic. Roy. Astron. Soc.*, **432** (1), 359—373. doi:10.1093/mnras/stt484.
99. Vavilova I. B., Ivashchenko G. Y., Babyk I. V., et al. (2015). The astrocosmic databases for multi-wavelength and cosmological properties of extragalactic sources. *Space Sci. & Technol.*, **21** (3), 94—107. doi:10.15407/knit2015.05.094.
100. Guo R., Hao C.-N., Xia X., et al. (2020). Toward an understanding of the massive red spiral galaxy formation. *Astrophys. J.*, **897** (2), 162. doi:10.3847/1538-4357/ab9b75.
101. Mezcua M., Lobanov A. P., Mediavilla E., Karouzos M. (2014). Photometric decomposition of mergers in disk galaxies. *Astrophys. J.*, **784** (1), 16. doi:10.1088/0004-637X/784/1/16.
102. Simmons B. D., Lintott C., Willett K. W., et al. (2017). Galaxy Zoo: Quantitative visual morphological classifications for 48 000 galaxies from CANDELS. *Mon. Notic. Roy. Astron. Soc.*, **464** (4), 4420—4447. doi:10.1093/mnras/stw2587.
103. Bottrell C., Hani M. H., Teimoorinia H., et al. (2019). Deep learning predictions of galaxy merger stage and the importance of observational realism. *Mon. Notic. Roy. Astron. Soc.*, **490** (4), 5390—5413. doi:10.1093/mnras/stz2934.
104. Pearson W. J., Wang L., Trayford J. W. Petrillo E., van der Tak F. F. S. (2019). Identifying galaxy mergers in observations and simulations with deep learning. *Astron. and Astrophys.*, **626**, A49. doi:10.1051/0004-6361/201935355.
105. Cabrera-Vives G., Miller C. J., Schneider J. Systematic labeling bias in galaxy morphologies. *Astron. J.*, **156** (6), 284. doi:10.3847/1538-3881/aae9f4.
106. Hart R. E., Bamford S. P., Willett K. W., et al. (2016). Galaxy Zoo: comparing the demographics of spiral arm number and a new method for correcting redshift bias. *Mon. Notic. Roy. Astron. Soc.*, **461** (4), 3663—3682. doi:10.1093/mnras/stw1588.
107. Tarsitano F., Bruderer C., Schawinski K., Hartley W. G. (2022). Image feature extraction and galaxy classification: a novel and efficient approach with automated machine learning. *Mon. Notic. Roy. Astron. Soc.*, **511** (3), 3330—3338. doi:10.1093/mnras/stac233.
108. Gauthier A., Jain A., Noordeh E. (2016). Galaxy Morphology Classification. e-proceedings, 1—6. URL: http://cs229.stanford.edu/proj2016/report/GauthierJainNoordeh-GalaxyMorphology-report.pdf (Last accessed: 30.09.2022).
109. Barchi P. H., de Carvalho R. R., Rosa R. R., et al. (2020). Machine and Deep Learning applied to galaxy morphology. A comparative study. *Astron. Comp.*, **30**, 100334. doi:10.1016/j.ascom.2019.100334.
110. Mittal A., Soorya A., Nagrath P., Hemanth D. J. (2020). Data augmentation based morphological classification of galaxies using deep convolutional neural network. *Earth Sci. Inform.*, **13**, 601—617. doi:10.1007/s12145-019-00434-8.
111. Sreejith S., Pereverzyev J., Kelvin L. S., et al. (2018). Galaxy and mass assembly: Automatic morphological classification of galaxies using statistical learning. *Mon. Notic. Roy. Astron. Soc.*, **474** (4), 5232—5258. doi:10.1093/mnras/stx2976.
112. Ghosh A., Urry C. M., Wang Z., et al. (2020). Galaxy morphology network: A convolutional neural network used to study morphology and quenching in ~100,000 SDSS and ~20,000 CANDELS galaxies. *Astrophys. J.*, **895** (2), 112. doi:10.3847/1538-4357/ab8a47.
113. Walmsley M., Scaife A. M. M., Lintott C., et al. (2022). Practical galaxy morphology tools from deep supervised representation learning. *Mon. Notic. Roy. Astron. Soc.*, **513** (2), 1581—1599. doi:10.1093/mnras/stac525.
114. Gauci A., Zarb Adami K., Abela J. (2010). *Machine learning for galaxy morphology classification*. arXiv:1005.0390.
115. Dom´ınguez S´anchez H., Huertas-Company M., Bernardi M., et al. (2018). Improving galaxy morphologies for SDSS with deep learning. *Mon. Notic. Roy. Astron. Soc.*, **476** (3), 3661—3676. doi:10.1093/mnras/sty338.
116. Yao-Yu Lin J., S.-M. Liao, Huang H.-J., et al. (2021). *Galaxy morphological classification with efficient vision transformer*. arXiv:2110.01024.
117. Karachentseva V. E., Vavilova I. B. (1994). Clustering of low surface brightness dwarf galaxies. I. General properties. *Bull. SAO*, **37**, 98—118.
118. Karachentseva V. E., Vavilova I. B. (1995). Clustering of dwarf galaxies with low surface brightness. II. The Virgo cluster. *Kinematics and Phys. Celestial Bodies.*, **11** (5), 38—48.
119. Sabatini S., Roberts S., Davies J. (2003). Dwarf LSB galaxies and their environment: The Virgo cluster, the Ursa Major cluster, isolated galaxies and voids. *Astrophys. J. Supl. Ser.*, **285** (1), 97—106. doi:10.1023/A:1024609809391.
120. Du W., Cheng C., Wu H., et al. (2019). Low Surface Brightness Galaxy catalogue selected from the .40-SDSS DR7 Survey and Tully-Fisher relation. *Mon. Notic. Roy. Astron. Soc.*, **483** (2), 1754—1795. doi:10.1093/mnras/sty2976.
121. Zhu X.-P., Dai J.-M., Bian C. J., et al. (2019). Galaxy morphology classification with deep convolutional neural networks. *Astrophys. Space Sci.*, **364** (4), 55. doi:10.1007/s10509-019-3540-1.

122. Dhar S., Shamir L. (202). Systematic biases when using deep neural networks for annotating large catalogs of astronomical images. *Astron. Comp.*, **38**, 100545. doi:10.1016/j.ascom.2022.100545.
123. Smethurst R. J., Masters K. L., Simmons B. D., et al. (2022). Quantifying the poor purity and completeness of morphological samples selected by galaxy colour. *Mon. Notic. Roy. Astron. Soc.*, **510** (3), 4126—4133. doi:10.1093/mnras/stab3607.
124. Kautsch S. J., Grebel E. K., Barazza F. D., et al. (2006). A catalog of edge-on disk galaxies. From galaxies with a bulge to superthin galaxies. *Astron. and Astrophys.*, **445** (2), 765—778. doi:10.1051/0004-6361:20053981.
125. Bizyaev D. V., Kautsch S. J., Mosenkov A. V., et al. (2014). The catalog of edge-on disk galaxies from SDSS. I. The catalog and the structural parameters of stellar disks. *Astrophys. J.*, **787** (1), 24. doi:10.1088/0004-637X/787/1/24.
126. Lima-Dias C., Monachesi A., Torres-Flores S., et al. (2021). An environmental dependence of the physical and structural properties in the Hydra cluster galaxies. *Mon. Notic. Roy. Astron. Soc.*, **500** (1), 1323—1339. doi:10.1093/mnras/staa3326.
127. Domínguez-Sánchez H., Huertas-Company M., Bernardi M., et al. (2019). Transfer learning for galaxy morphology from one survey to another. *Mon. Notic. Roy. Astron. Soc.*, **484** (1), 93—100. doi:10.1093/mnras/sty3497.
128. Lingard T. K., Masters K. L., Krawczyk C., et al. (2020). Galaxy Zoo builder: Four-component photometric decomposition of spiral galaxies guided by citizen science. *Astrophys. J.*, **900** (2), 178. doi:10.3847/1538-4357/ab9d83.
129. Schawinski K., Urry C. M., Simmons B. D., et al. (2014). The green valley is a red herring: Galaxy Zoo reveals two evolutionary pathways towards quenching of star formation in early- and late-type galaxies. *Mon. Notic. Roy. Astron. Soc.*, **440** (1), 889—907. doi:10.1093/mnras/stu327.
130. Madore B. F., Nelson E., Petrillo K. (2009). VizieR Online Data Catalog: Collisional ring galaxies atlas (Madore+, 2009). VizieR Online Data Catalog (2009) J/ApJS/181/572.
131. Smirnov D. V., Reshetnikov V. P. (2022). *The luminosity function of ringed galaxies*. arXiv:2209.06875.
132. Hoyle B., Masters K. L., Nichol R. C., et al. (2011). Galaxy Zoo: bar lengths in local disc galaxies. *Mon. Notic. Roy. Astron. Soc.*, **415** (4), 3627—3640. doi:10.1111/j.1365-2966.2011.18979.x.
133. Reza M. (2021). Galaxy morphology classification using automated machine learning. *Astron. Comp.*, **37**, 100492. doi: 10.1016/j.ascom.2021.100492.
134. Vavilova I. B., Karachentseva V. E., Makarov D. I., Melnyk O. V. (2005). Triplets of galaxies in the local supercluster. I. Kinematic and virial parameters.*Kinematics and Phys. Celestial Bodies*, **21** (1), 3—20.
135. Darg D. W., Kaviraj S., Lintott C. J., et al. (2010). Galaxy Zoo: The fraction of merging galaxies in the SDSS and their morphologies. *Mon. Notic. Roy. Astron. Soc.*, **401** (2), 1043—1056. doi:10.1111/j.1365-2966.2009.15686.x.
136. Weston M. E., McIntosh D. H., Brodwin M., et al. Incidence of WISE-selected obscured AGNs in major mergers and interactions from the SDSS. *Mon. Notic. Roy. Astron. Soc.*, **464** (4), 3882—3906. doi:10.1093/mnras/stw2620.
137. Pearson W. J., Suelves L. E., Ho S. C. C., et al. (2022). North Ecliptic Pole merging galaxy catalogue. *Astron. and Astrophys.*, **661**, A52. doi:10.1051/0004-6361/202141013.
138. Ahn C. P., Alexandroff R., Allende Prieto C., et al. (2012). The Ninth Data Release of the Sloan Digital Sky Survey: First Spectroscopic Data from the SDSS-III Baryon Oscillation Spectroscopic Survey. *Astrophys. J. Supl.*, **203** (2), 21. doi:10.1088/0067-0049/203/2/21.
139. Blanton M. R., Bershady M. A., Abolfathi B., et al. (2017). SDSS IV: Mapping the Milky Way, nearby galaxies, and the distant universe. *Astron. J.,* **154**, 28. doi:10.3847/1538-3881/aa7567.
140. Wenger M., Ochsenbein F., Egret D., et al. (2000). The SIMBAD astronomical database. The CDS reference database for astronomical objects. *Astron. and Astrophys. Supl.*, **143**, 9—22. doi:10.1051/aas:2000332.

Стаття надійшла до редакції	*22.09.2022*	*Received 22.09.2022*
Після доопрацювання	*29.09.2022*	*Revised 29.09.2022*
Прийнято до друку	*02.10.2022*	*Accepted 02.10.2022*

В. Храмцов[1], аспірант
https://orcid.org/0000-0003-1744-7071
E-mail: vld.khramtsov@gmail.com
І. Б. Вавилова[2], зав. відділу, д-р фіз.-мат. наук, проф.
https://orcid.org/0000-0002-5343-1408
E-mail: irivav@mao.kiev.ua
Д. В. Добричева[2], старш. наук. співроб., канд. фіз.-мат. наук,
https://orcid.org/0000-0001-5557-3453
E-mail: daria@mao.kiev.ua
М. Ю. Василенко[2], аспірант
https://orcid.org/0000-0002-7714-0779
E-mail: vasmax@mao.kiev.ua
О. В. Мельник[2], старш. наук. співроб., канд. фіз.-мат. наук
E-mail: melnykol@gmail.com
А. А. Елиїв[2], старш. наук. співроб., канд. фіз.-мат. наук
https://orcid.org/ 0000-0001-6215-1048
E-mail: andrii.elyiv@gmail.com
В. С. Ахметов[1], заст. дир. з наук. роботи, канд. фіз.-мат. наук
E-mail: akhmetovvs@gmail.com
А. М. Дмитренко[1], аспірант
E-mail: astronom.karazin007@gmail.com

[1] НДІ астрономії, Харківський національний університет ім. В. Н. Каразіна
вул. Сумська 35, Харків, Україна, 61022
[2] Головна астрономічна обсерваторія НАН України
вул. Академіка Заболотного 27, Київ, Україна, 03143

МАШИННЕ НАВЧАННЯ ДЛЯ МОРФОЛОГІЧНОЇ КЛАСИФІКАЦІЇ ГАЛАКТИК ІЗ ОГЛЯДУ SDSS. III. ДЕТАЛЬНІ ХАРАКТЕРИСТИКИ ЗА ОБРОБКОЮ ЗОБРАЖЕНЬ У ЗГОРТКОВІЙ НЕЙРОННІЙ МЕРЕЖІ

Стаття є продовженням наших робіт із застосування різних методів машинного навчання до морфологічної класифікації галактик (Vavilova et al., 2021, 2022). Ми досліджували вибірку ~315 800 SDSS DR9 галактик із абсолютними зоряними величинами $-24^m < M_r < -19.4^m$ на червоних зміщеннях $0.003 < z < 0.1$ як цільову вибірку даних для CNN класифікатора. Оскільки цільова вибірка тісно перетинається із Galaxy Zoo 2 (GZ2), ми використовуємо ці анотовані дані як навчальну вибірку для класифікації галактик за 34 детальними морфологічними характеристиками. За наявності вираженої різниці у яскравості і розмірах між галактиками з навчальної вибірки і галактиками без відомих морфологічних параметрів ми застосували нові методики, які дозволили нам вперше позбутися цієї різниці для менших і слабкіших галактик SDSS із $m_r < 17.7$. У статті детально описано ці методи змагальної перевірки, а також процедури оптимального розподілу галактик із тренувальної вибірки для перевірки CNN-моделі на основі DenseNet-201. Ми також знайшли оптимальні трансформації зображень галактик (зміна яскравості, повороти, підгонка розмірів тощо), які допомагають покращити ефективність CNN-класифікатора у пошуку подібності зображень.

Це можна розглядати як ще один спосіб покращити точність морфологічної деталізації зображень галактик, для яких вона була статистично низькою в проєкті GZ. Такий підхід, подібно до аутоімунізації, коли CNN-класифікатор, навчений на дуже хороших зображеннях, здатний перенавчити погані зображення з тієї самої однорідної вибірки, можна вважати аналогічним іншим методам покращення байєса. Найбільш багатообіцяючий результат щодо ймовірності CNN-прогнозування отримано для таких морфологічних характеристик галактик як кільця, бар, балдж, ознаки взаємодії, іррегулярності тощо, – точність становить від 83.3 до 99.4 % за винятком характеристик «порушена структура» (68.55 %) і «середня закрутка спіральних рукавів» (77.39 %).

У результаті ми вперше визначили детальну морфологічну класифікацію для більш ніж 140 000 галактик на $z < 0.1$, переважна більшість яких має низьку яскравість. Візуальна перевірка вибірок галактик з певними морфологічними ознаками дозволила виявити типові проблемні точки CNN-класифікації зображень галактик з астрономічної точки зору.

Морфологічні каталоги галактик SDSS із найцікавішими морфологічними особливостями доступні на веб-сайті УкрВО (http://ukr-vo.org/galaxies/) та VizieR.

Ключові слова: галактики, морфологічна класифікація, методи: аналіз даних, згорткова нейронна мережа (CNN), обробка зображень.